

Fall 9-23-2015

# Evaluation of Anisole-Substituted Boron Difluoride Formazanate Complexes for Fluorescence Cell Imaging

Ryan R. Maar

Stephanie M. Barbon

Neha Sharma

Hilary Groom

Leonard G. Luyt

*See next page for additional authors*

Follow this and additional works at: <https://ir.lib.uwo.ca/chempub>

 Part of the [Chemistry Commons](#)

---

## Citation of this paper:

Maar, Ryan R.; Barbon, Stephanie M.; Sharma, Neha; Groom, Hilary; Luyt, Leonard G.; and Gilroy, Joe, "Evaluation of Anisole-Substituted Boron Difluoride Formazanate Complexes for Fluorescence Cell Imaging" (2015). *Chemistry Publications*. 69.  
<https://ir.lib.uwo.ca/chempub/69>

---

**Authors**

Ryan R. Maar, Stephanie M. Barbon, Neha Sharma, Hilary Groom, Leonard G. Luyt, and Joe Gilroy

# Evaluation of Anisole-Substituted Boron Difluoride Formazanate Complexes for Fluorescence Cell Imaging

Ryan R. Maar,<sup>[a,b]</sup> Stephanie M. Barbon,<sup>[a,b]</sup> Neha Sharma,<sup>[a]</sup> Hilary Groom,<sup>[c]</sup> Leonard G. Luyt,<sup>\*[a,c,d]</sup> and Joe B. Gilroy<sup>\*[a,b]</sup>

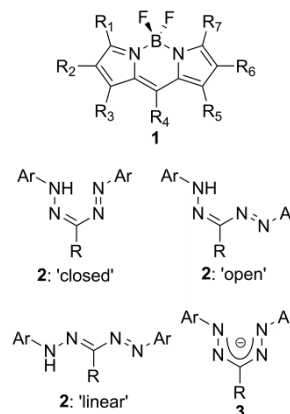
**Abstract:** The evaluation of three subclasses of boron difluoride formazanate complexes bearing *o*-, *m*-, and *p*-anisole *N*-aryl substituents (Ar) as readily accessible alternatives to boron dipyrromethene (BODIPY) dyes for cell imaging applications is described. While the wavelengths of maximum absorption ( $\lambda_{\text{max}}$ ) and emission ( $\lambda_{\text{em}}$ ) observed for each subclass of complexes, which differed by their carbon-bound substituents (R), were similar, the emission quantum yields for **7a–c** (R = cyano) were enhanced relative to **8a–c** (R = nitro) and **9a–c** (R = phenyl). Complexes **7a–c** and **8a–c** were also significantly easier to reduce electrochemically to their radical anion and dianion forms compared to **9a–c**. Within each subclass, the *o*-substituted derivatives were more difficult to reduce, had shorter  $\lambda_{\text{max}}$  and  $\lambda_{\text{em}}$ , and lower emission quantum yields than the *p*-substituted analogs as a result of sterically-driven twisting of the *N*-aryl substituents and a decrease in the degree of  $\pi$  conjugation. The *m*-substituted complexes were the least difficult to reduce and possessed intermediate  $\lambda_{\text{max}}$ ,  $\lambda_{\text{em}}$ , and quantum yields. The complexes studied also exhibited large Stokes shifts (82–152 nm, 2143–5483  $\text{cm}^{-1}$ ). Finally, the utility of complex **7c** (Ar = *p*-anisole, R = cyano), which can be prepared for just a few dollars per gram, for fluorescence cell imaging was demonstrated. The use of **7c** and 4',6-diamino-2-phenylindole (DAPI) allowed for simultaneous imaging of the cytoplasm and nucleus of mouse fibroblast cells.

## Introduction

Boron difluoride ( $\text{BF}_2$ ) chelates of *N*-donor ligands are among the most widely studied classes of molecular materials due to their unique, tunable, and potentially useful absorption, emission, and electrochemical properties.<sup>[1],[2]</sup> These compounds, including the ubiquitous boron dipyrromethanes (BODIPYs) **1**,<sup>[3]</sup> have shown utility as sensors,<sup>[4],[5]</sup> as efficient electrochemiluminescence luminophores,<sup>[6],[7]</sup> as the functional component of organic electronics,<sup>[8]</sup> in photodynamic

therapy,<sup>[9],[10]</sup> and perhaps most commonly, as fluorescence cell imaging agents.<sup>[11],[12]</sup> Despite their widespread use in a broad range of applications, further development of the chemistry of many  $\text{BF}_2$  complexes has often been limited by their challenging synthesis and/or substantial cost. For example, a few milligrams of commercially available BODIPYs for cell imaging applications will often cost several hundred US dollars. Considering these factors, there remains a significant need for readily accessible molecular materials with similar or improved properties compared to BODIPYs that may be prepared via relatively simple, low-cost synthetic pathways.

$\text{BF}_2$  formazanate complexes meet these criteria and offer the ability to tune spectroscopic and electrochemical properties through structural variation.<sup>[13]</sup> The parent formazans **2**,<sup>[14]</sup> known primarily for their use in cell viability assays,<sup>[15]</sup> are typically prepared using aryl diazonium coupling reactions in aqueous media. They exist in three different conformations (*i.e.*, 'closed', 'open', or 'linear') depending on the carbon-bound substituent (R) present.<sup>[14a, 16]</sup> In recent years, the coordination chemistry of formazanate ligands **3** has received significant attention due to the rich spectroscopic and redox properties exhibited by the resulting complexes.<sup>[17],[18]</sup> However, their utility in practical applications such as cell imaging has not been demonstrated.



Herein, taking inspiration from the biocompatibility of formazans, we present a study designed to evaluate a series of anisole-substituted  $\text{BF}_2$  formazanate complexes (Ar = *o*-anisole, *m*-anisole, *p*-anisole; R = cyano, nitro, phenyl) in an effort to showcase their utility as fluorescence cell imaging agents.

## Results and Discussion

### Synthesis

Anisole-substituted formazans **4a–c**, **5a–c**, and **6a–c** were prepared by adapting established procedures for the coupling of aryl diazonium salts and activated methylenes such as cyanoacetic acid, nitromethane, and phenylpyruvic acid in yields ranging from 18–90%.<sup>[16, 19]</sup> It is worth noting that the variability in

- [a] R.R. Maar, S.M. Barbon, N. Sharma, Prof. Dr. L.G. Luyt, and Prof. Dr. J.B. Gilroy  
Department of Chemistry  
The University of Western Ontario  
1151 Richmond St. N., London, Ontario N6A 5B7 (Canada)  
E-mail: lluyt@uwo.ca, joe.gilroy@uwo.ca
- [b] R.R. Maar, S.M. Barbon, and Prof. Dr. J.B. Gilroy  
The Centre for Advanced Materials and Biomaterials Research (CAMBR)  
The University of Western Ontario  
1151 Richmond St. N., London, Ontario N6A 5B7 (Canada)
- [c] H. Groom and Prof. Dr. L.G. Luyt  
Department of Oncology, London Regional Cancer Program  
790 Commissioners Rd. E., London, Ontario N6A 4L6 (Canada)
- [d] Prof. Dr. L.G. Luyt  
Department of Medical Imaging  
The University of Western Ontario  
1151 Richmond St. N., London, Ontario N6A 5B7 (Canada)

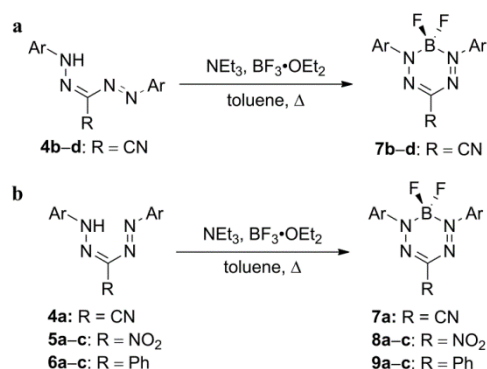
Supporting information for this article is given via a link at the end of the document.

reaction yields relates mainly to the unpredictable stability of the aryl diazonium salts involved.<sup>[20]</sup> 3-Cyanoformazans **4b–d** exist primarily in the 'open' conformation in solution due to the presence of a linear carbon-bound cyano substituent and were identified by their characteristic orange color [wavelength of maximum absorption ( $\lambda_{\text{max}}$ ): 419–453 nm] and the chemical shift of the  $^1\text{H}$  NMR resonance originating from their NH protons ( $\delta$ : 11.75–12.89). All other formazans produced during this study exist in the more common 'closed' conformation in solution and exhibit characteristic NH resonances in their  $^1\text{H}$  NMR spectra between 13.91 and 15.56 ppm and  $\lambda_{\text{max}}$  values between 448 and 530 nm in their UV-vis absorption spectra.

$\text{BF}_2$  formazanate complexes **7a–d**, **8a–c**, and **9a–c** were prepared by heating the appropriate formazan in toluene with an excess of triethylamine and boron trifluoride diethyl etherate (Scheme 1, Table 1, Figures S1–S36). The isolated yields for the complexes ranged from 15–91% and were highly dependent on the purification methods employed. All new  $\text{BF}_2$  formazanate complexes were fully characterized by  $^1\text{H}$ ,  $^{11}\text{B}$ ,  $^{13}\text{C}$ , and  $^{19}\text{F}$  NMR spectroscopy, UV-vis absorption and emission spectroscopy, IR spectroscopy, and high-resolution mass spectrometry. The formation of the  $\text{BF}_2$  complexes was accompanied by the disappearance of the NH resonance in their  $^1\text{H}$  NMR spectra, and the appearance of a 1:2:1 triplet and a 1:1:1:1 quartet in their  $^{11}\text{B}$  and  $^{19}\text{F}$  NMR spectra, respectively. With the exception of **7a** (Ar = *o*-anisole, R = cyano), the  $\text{BF}_2$  complexes were stable towards hydrolysis. In the presence of 10 equivalents of water, complex **7a** slowly hydrolyzed to re-form the parent formazan **4a** (4% degradation after 48 h, 8% degradation after 96 h). By comparison, complex **7d** (Ar = *o*-ethylbenzene, R = cyano) was indefinitely stable towards hydrolysis under the same conditions. Based on this comparison, we conclude that the hydrolysis of **7a** is not driven by steric interactions alone, but rather that the lone pairs on oxygen likely play an important role in the decomposition pathway. Furthermore, the presence of the linear carbon-bound cyano substituent in **7a** may facilitate its decomposition as it potentially allows for 'open' and 'linear' ligand arrangements to be accessed. Similar ligand orientations are less likely for reaction intermediates derived from complexes **8a** and **9a**, which possess non-linear nitro and phenyl carbon-bound substituents.

### X-ray Crystallography

Single crystals of complexes **7a** and **7b** suitable for X-ray diffraction studies were grown by slow evaporation of saturated dichloromethane solutions in a sealed vessel containing hexanes. In the solid-state **7a** and **7b** exist in 'dragonfly' conformations, with the nitrogen-nitrogen and carbon-nitrogen bond lengths of the formazanate ligand backbone falling between those typically associated with single and double bonds of the same atoms (Figure 1, Table 2).<sup>[21]</sup> The *N*-aryl substituents are bent out of plane relative to the  $\text{N}_4$  backbone of the formazanate ligands by an average torsion angle of 61.2 and 47.7° for **7a** and **7b**, respectively. The boron atoms reside 0.54 and 0.50 Å out of the  $\text{N}_4$  plane in the structures of **7a** and **7b**.



**Scheme 1.** General synthetic approach for the synthesis of  $\text{BF}_2$  formazanate complexes **7b–d** (a) and  $\text{BF}_2$  formazanate complexes **7a**, **8a–c** and **9a–c** (b). See Table 1 for a detailed list of substituents.

**Table 1.** Substituents for formazans **4a–d**, **5a–c**, and **6a–c** and  $\text{BF}_2$  formazanate complexes **7a–d**, **8a–c**, and **9a–c**.

Compound	Ar	R
<b>4a/7a</b>	<i>o</i> -anisole	cyano
<b>4b/7b</b>	<i>m</i> -anisole	cyano
<b>4c/7c</b>	<i>p</i> -anisole	cyano
<b>4d/7d</b>	<i>o</i> -ethylbenzene	cyano
<b>5a/8a</b>	<i>o</i> -anisole	nitro
<b>5b/8b</b>	<i>m</i> -anisole	nitro
<b>5c/8c</b>	<i>p</i> -anisole	nitro
<b>6a/9a</b>	<i>o</i> -anisole	phenyl
<b>6b/9b</b>	<i>m</i> -anisole	phenyl
<b>6c/9c</b>	<i>p</i> -anisole	phenyl

These values are substantially larger than the torsion angles of 18.3 and 37.1° and boron displacements of 0.13 and 0.34 Å observed for the two crystallographically independent forms of **7c**.<sup>[13b]</sup> Initially, we were tempted to rationalize these trends through steric arguments, whereby interactions between the *o*-, and to a lesser extent, *m*-methoxy groups and the fluorine atoms may lead to twisting of the *N*-aryl substituents relative to the formazanate backbone. While this interpretation appears to hold true for **7a** (Ar = *o*-anisole, R = cyano), the large torsion angles observed for **7b** (Ar = *m*-anisole, R = cyano) likely arise due to crystal packing effects including slipped  $\pi$ -stacking interactions (Figure S37). This conclusion is further corroborated by the fact that the methoxy substituents are *anti* to the  $\text{BF}_2$  moiety in the solid-state structure of **7b**.

### Cyclic Voltammetry

The electrochemical properties of  $\text{BF}_2$  complexes **7a–c** were studied using cyclic voltammetry (Figure 2 and S38, Table 3). Each complex underwent two reversible one-electron reductions to form the corresponding ligand-centered radical anion and dianion (Scheme 2), while **7c** was the only complex in the series that was oxidized (irreversibly) within the electrochemical window offered by acetonitrile. We have previously shown that electron-donating *N*-aryl substituents render  $\text{BF}_2$  formazanate

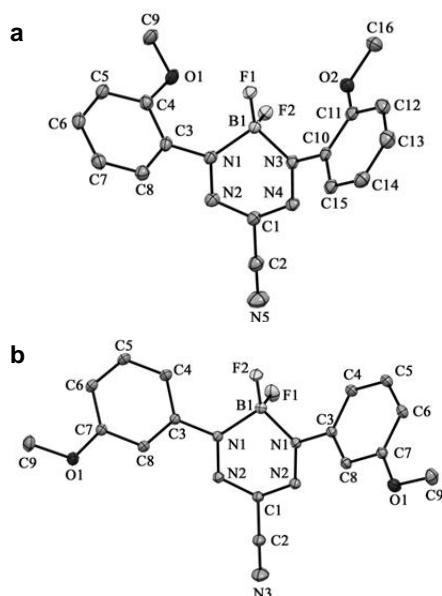


**Figure 1.** Solid-state structures of complexes **7a** (a) and **7b** (b). Anisotropic displacement ellipsoids are shown at 50% probability and hydrogen atoms have been omitted for clarity.

**Table 2.** Selected bond lengths (Å) and angles (deg) for BF<sub>2</sub> formazanate complexes **7a–c**.

	<b>7a</b>	<b>7b</b>	<b>7c</b> <sup>[a]</sup>	
N1–N2	1.3040(16)	1.2987(6)	1.307(2)	1.306(2)
N3–N4	1.3038(16)	–	1.304(2)	1.302(2)
C1–N2	1.3404(19)	1.3443(5)	1.340(3)	1.335(3)
C1–N4	1.3438(18)	–	1.335(3)	1.340(3)
N1–N2–C1	116.09(11)	116.42(4)	116.75(18)	116.21(17)
N1–B1–N3	101.99(10)	–	106.85(17)	104.75(16)
N1–B1–N1'	–	102.63(5)	–	–
N2–C1–N4	126.85(12)	–	130.0(2)	129.32(18)
N2'–C1–N2	–	127.22(6)	–	–
boron displacement <sup>[b]</sup>	0.54	0.50	0.13	0.34
dihedral angles <sup>[c]</sup>	62.0, 60.5	47.7, 47.7	15.3, 21.4	37.6, 36.6

[a] The asymmetric unit determined for BF<sub>2</sub> complex **7c** contains two unique molecules. [b] Distance between B1 and the N<sub>4</sub> plane. [c] Torsion angle between N1 and N3 aryl substituents and the N<sub>4</sub> plane.

complexes more difficult to reduce than the phenyl-substituted analogs, and that the opposite is true for complexes bearing electron-withdrawing substituents.<sup>[13b, c]</sup> In the present study, the interpretation is slightly more complex as both steric and electronic effects must be considered. Complexes **7a** and **7c** possess anisole substituents with *o*- and *p*-substitution patterns, which potentially allow for resonance donation of oxygen lone pairs leading to extended  $\pi$  conjugation of the formazanate framework. The *m*-substituted complex **7b** is not resonance delocalized, and should therefore possess properties purely associated with the inductive electron-withdrawing character of the methoxy group. Indeed, **7b** is the easiest complex to reduce within the series ( $E^{\circ}_{\text{red1}} = -0.50$  V;  $E^{\circ}_{\text{red2}} = -1.62$  V vs. ferrocene/ferrocenium). The *o*-substituted complex **7a** was

observed to be more difficult to reduce ( $E^{\circ}_{\text{red1}} = -0.73$  V;  $E^{\circ}_{\text{red2}} = -1.88$  V) than the *p*-substituted complex **7c** ( $E^{\circ}_{\text{red1}} = -0.68$  V;  $E^{\circ}_{\text{red2}} = -1.82$  V). We attribute this behavior to twisting of the *o*-anisole substituents relative to the formazanate backbone in **7a** in solution. This twisting, which is consistent with the solid-state structure described above, limits the degree of  $\pi$  conjugation of the formazanate framework. The reduced degree of  $\pi$  conjugation results in destabilization of the lowest unoccupied molecular orbital (LUMO), and, in turn, renders **7a** more difficult to reduce than the  $\pi$  conjugated complex **7c**. This argument is supported by DFT studies that showed the LUMO orbital of closely related complexes to include both the formazanate backbone and *N*-aryl substituents.<sup>[13b, 13d]</sup> In order to confirm that the effect of the substituent pattern on the electrochemical properties of anisole-substituted BF<sub>2</sub> formazanate complexes was general, cyclic voltammograms were also collected for **8a–c** (R = nitro) and **9a–c** (R = phenyl) (Figures S39 and S40, Table 3). Nitro-substituted complexes **8a–c** were slightly easier to reduce than the corresponding cyano-substituted complexes due to the strong electron-withdrawing nature of the nitro group, while phenyl-substituted complexes **9a–c** were much more difficult to reduce due to the absence of a strongly electron-withdrawing carbon-bound substituent on the formazanate backbone. For each series, the *m*-substituted complexes were the easiest to reduce and the *o*-substituted complexes were more difficult to reduce than the *p*-analogs, confirming that the trend discussed above is general.

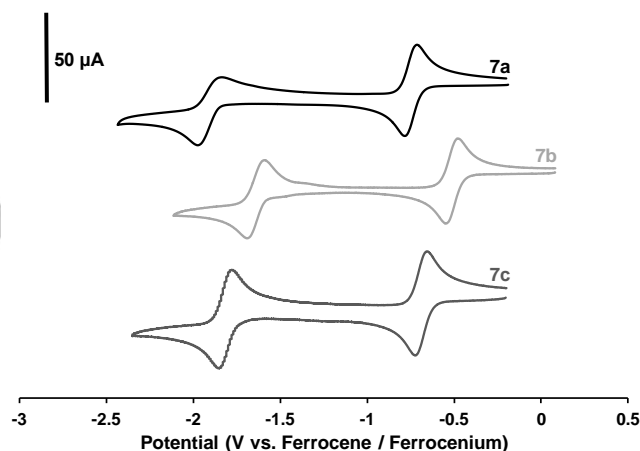
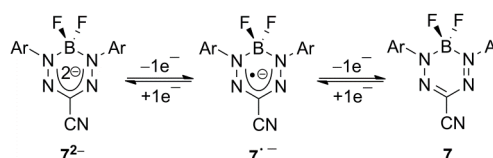


**Figure 2.** Cyclic voltammograms for BF<sub>2</sub> formazanate complexes **7a** (Ar = *o*-anisole, R = cyano), **7b** (Ar = *m*-anisole, R = cyano), and **7c** (Ar = *p*-anisole, R = cyano) recorded in dry, degassed acetonitrile containing ~1 mM analyte and 0.1 M *n*-Bu<sub>4</sub>NPF<sub>6</sub> at a scan rate of 100 mV s<sup>-1</sup>.



**Scheme 2.** Electrochemical reduction of BF<sub>2</sub> formazanate complexes **7a**, **7b**, and **7c** (Ar = *o*-anisole, *m*-anisole, or *p*-anisole).

Table 3. Solution characterization data for BF<sub>2</sub> complexes **7a–d**, **8a–c**, and **9a–c**.

	solvent	$\lambda_{\max}$ (nm)	$\epsilon$ (M <sup>-1</sup> cm <sup>-1</sup> )	$\lambda_{\text{em}}$ (nm)	$\Phi_{\text{f}}^a$	$\nu_{\text{ST}}$ (nm)	$\nu_{\text{ST}}$ (cm <sup>-1</sup> )	$E_{\text{red1}}^{\text{c}}$ (V)	$E_{\text{red2}}^{\text{c}}$ (V)
<b>R = cyano</b>									
<b>7a</b> (Ar = <i>o</i> -anisole)	THF	456	10,100	590	0.03	134	4981		
	CH <sub>2</sub> Cl <sub>2</sub>	466	15,500	589	0.04	123	4481	-0.73	-1.88
	toluene	467	16,000	592	0.05	125	4521		
<b>7b</b> (Ar = <i>m</i> -anisole)	THF	510	20,000	639	0.01	129	3958		
	CH <sub>2</sub> Cl <sub>2</sub>	517	18,500	637	0.03	120	3644	-0.50	-1.62
	toluene	525	21,100	635	0.13	110	3300		
<b>7c</b> <sup>[13b]</sup> (Ar = <i>p</i> -anisole)	THF	556	33,400	662	0.46	106	2880		
	CH <sub>2</sub> Cl <sub>2</sub>	558	35,300	661	0.65	103	2793	-0.68	-1.82
	toluene	572	42,700	656	0.77	84	2239		
<b>7d</b> (Ar = <i>o</i> -ethylbenzene)	THF	433	12,000	562	0.01	129	5301		
	CH <sub>2</sub> Cl <sub>2</sub>	431	14,300	562	0.02	131	5408	-0.66	-1.86
	toluene	436	14,000	565	0.02	129	5236		
<b>R = nitro</b>									
<b>8a</b> (Ar = <i>o</i> -anisole)	THF	456	5,900	608	0.03	152	5483		
	CH <sub>2</sub> Cl <sub>2</sub>	466	7,100	599	0.03	133	4768	-0.71	-1.83
	toluene	468	7,500	603	0.05	135	4784		
<b>8b</b> (Ar = <i>m</i> -anisole)	THF	512	17,700	656	<0.01	144	4287		
	CH <sub>2</sub> Cl <sub>2</sub>	511	18,300	651	<0.01	140	4209	-0.43	-1.54
	toluene	533	18,400	644	0.04	111	3234		
<b>8c</b> (Ar = <i>p</i> -anisole)	THF	559	26,700	667	0.17	108	2897		
	CH <sub>2</sub> Cl <sub>2</sub>	564	20,100	665	0.24	101	2693	-0.60	-1.72
	toluene	572	23,600	661	0.33	82	2143		
<b>R = phenyl</b>									
<b>9a</b> (Ar = <i>o</i> -anisole)	THF	459	18,900	592	<0.01	133	4895		
	CH <sub>2</sub> Cl <sub>2</sub>	464	21,600	588	0.01	124	4545	-1.09	-1.97
	toluene	467	18,800	596	<0.01	129	4635		
<b>9b</b> (Ar = <i>m</i> -anisole)	THF	520	25,000	643	<0.01	123	3679		
	CH <sub>2</sub> Cl <sub>2</sub>	521	25,000	644	0.025	123	3666	-0.81	-1.87
	toluene	530	22,900	644	0.012	114	3340		
<b>9c</b> (Ar = <i>p</i> -anisole)	THF	548	23,400	672	0.019	124	3367		
	CH <sub>2</sub> Cl <sub>2</sub>	545	29,300	670	0.063	125	3423	-0.94	-1.93
	toluene	551	25,500	672	0.028	121	3268		

<sup>a</sup>Quantum yields were determined according to a published protocol<sup>[22b]</sup> using ruthenium tris(bipyridine) hexafluorophosphate as a relative standard<sup>[22b]</sup> and corrected for wavelength-dependent detector sensitivity (Figure S41). <sup>b</sup>Cyclic voltammograms were recorded in dry, degassed acetonitrile containing ~1 mM analyte and 0.1 M *n*-Bu<sub>4</sub>NPF<sub>6</sub> at a scan rate of 100 mV s<sup>-1</sup> and internally referenced relative to the ferrocene/ferrocenium redox couple.

### UV-vis Absorption and Emission Spectroscopy

The UV-vis absorption and emission spectra for BF<sub>2</sub> complexes **7a–c** (R = cyano) are shown in Figure 3 and the data summarized in Table 3. Each of the complexes is strongly absorbing within the visible region of the electromagnetic spectrum with wavelengths of maximum absorption ( $\lambda_{\max}$ ) ranging from 467 to 572 nm and molar extinction coefficients ( $\epsilon$ ) ranging from 16,000 to 42,700 M<sup>-1</sup> cm<sup>-1</sup> in toluene. The low-energy absorption maxima for a similar set of complexes was shown by time-dependent DFT to involve primarily the highest occupied molecular orbital (HOMO)-LUMO transition.<sup>[13d]</sup> The same series of compounds exhibited wavelengths of maximum emission ( $\lambda_{\text{em}}$ ) ranging from 592 to 656 nm and quantum yields ( $\Phi_{\text{f}}$ ) ranging from 0.05 to 0.77. As a result of the twisted conformation adopted by the *N*-aryl substituents, and the reduced degree of  $\pi$  conjugation that results, the *o*-substituted complex **7a** had the lowest values of  $\lambda_{\max}$  (467 nm),  $\epsilon$  (16,000 M<sup>-1</sup> cm<sup>-1</sup>),  $\lambda_{\text{em}}$  (592 nm), and  $\Phi_{\text{f}}$  (0.05). Conversely, *p*-substituted complex **7c** possessed properties consistent with extended  $\pi$  conjugation arising from the relatively coplanar orientation of the *N*-aryl substituents and the formazanate backbone ( $\lambda_{\max}$  = 572 nm;  $\epsilon$  = 42,700 M<sup>-1</sup> cm<sup>-1</sup>;  $\lambda_{\text{em}}$  = 656 nm; and  $\Phi_{\text{f}}$  = 0.77). The spectroscopic characteristics of the *m*-substituted analog **7b** fall between those observed for **7a** and **7c** and are dictated by the presence of the inductively electron-withdrawing methoxy group ( $\lambda_{\max}$  = 525 nm;  $\epsilon$  = 21,100 M<sup>-1</sup> cm<sup>-1</sup>;  $\lambda_{\text{em}}$  = 635 nm; and  $\Phi_{\text{f}}$  = 0.13). Complex **7d**, which has *o*-ethylbenzene *N*-aryl substituents, has  $\lambda_{\max}$  = 436 nm and  $\epsilon$  = 14,000 M<sup>-1</sup> cm<sup>-1</sup>,

confirming that the twisted structure postulated for **7a** is not unique to anisole-substituted compounds, and is driven by steric interactions (Figure S42). The spectroscopic properties

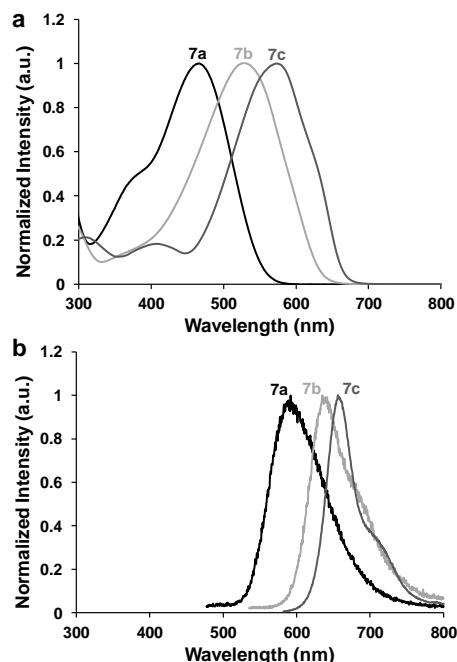


**Figure 3.** UV-vis absorption spectra (a) and emission spectra (b) for BF<sub>2</sub> formazanate complexes **7a** (Ar = *o*-anisole, R = cyano), **7b** (Ar = *m*-anisole, R = cyano), and **7c** (Ar = *p*-anisole, R = cyano) recorded for degassed 10  $\mu$ M toluene solutions.

observed for complexes **8a–c** (R = nitro) and **9a–c** (R = phenyl) were closely related to those of **7a–c**, further demonstrating the generality of the trend observed (Figures S43 and S44). However, it must be noted that the emission quantum yields calculated for **8a–c** and **9a–c**, were lower than those calculated for **7a–c**. In particular, **9a–c** are weakly emissive, likely as a result of non-radiative decay pathways associated with the carbon-bound phenyl substituent. Each of the anisole-substituted BF<sub>2</sub> complexes reported in this study exhibited large Stokes shifts ( $\nu_{ST}$ ) ranging from 82 to 152 nm (2143–5483 cm<sup>-1</sup>). This key characteristic of BF<sub>2</sub> formazanate complexes is of significant importance to their potential use as fluorescence cell imaging agents, where photon re-absorption greatly limits emission intensity.

### Cell Imaging

Based on our evaluation of the anisole-substituted BF<sub>2</sub> formazanate complexes described above, we concluded that complex **7c**, which can be prepared in two straightforward synthetic steps involving minimal bench time for just a few dollars per gram, was an excellent candidate for fluorescence cell-imaging studies. To this end, the uptake of complex **7c** into fibroblast cells was investigated (Figure 4).

Mouse fibroblast cells were incubated with **7c** for one hour, and after washing and fixing, were imaged by confocal fluorescence microscopy.

The fluorescence images demonstrated that **7c** was internalized by the fibroblast cells (Figure 4a,b). As a result of the low-energy ( $\lambda_{em}$  ~660 nm) emission of **7c**, this dye proved to be well suited for orthogonal imaging applications. We explored this potential by co-staining cells with the nuclear dye 4',6-diamidino-2-phenylindole (DAPI), and demonstrated that **7c** and DAPI could be used to image the cell cytoplasm and nucleus simultaneously (Figure 4c,d). During the course of these studies, we frequently observed punctate staining, which could be due to the dye being localized in either the endoplasmic reticulum and/or vesicles. Aggregation of the dye could be another possible explanation for the punctate appearance. However, we were able to rule out aggregation induced emission enhancement by adding water to tetrahydrofuran solutions of **7c**, and demonstrating that emission intensity decreases as the volume fraction of water is increased and aggregates begin to form (Figure S45). We therefore conclude that the punctate staining is due to high local concentration of **7c** rather than aggregation.

### Conclusions

We have systematically evaluated a library of *o*-, *m*-, and *p*-anisole-substituted BF<sub>2</sub> formazanate complexes, and, for the first time, demonstrated their potential as readily accessible fluorescence imaging agents. The substitution pattern for each

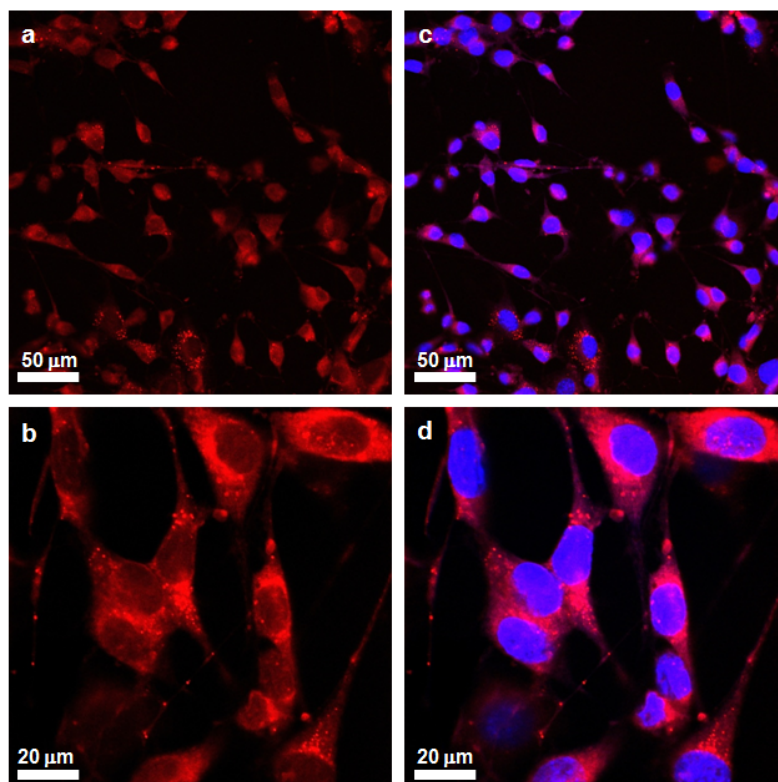


**Figure 4.** Confocal fluorescence micrographs of mouse fibroblast cells stained with BF<sub>2</sub> formazanate complex **7c** and DAPI. Images (a) and (b) were visualized with excitation at 559 nm and emission collected between 625–725 nm. Images (c) and (d) are an overlay of images (a) and (b) with those obtained from excitation at 405 nm and emission collected between 425–475 nm.

subset of complexes (R = cyano, nitro, and phenyl) was shown to have a dramatic effect on their electrochemical and spectroscopic properties. In each case, the *o*-substituted complexes were the most difficult to reduce electrochemically, had the shortest  $\lambda_{\text{max}}$  and  $\lambda_{\text{em}}$ , and possessed low emission quantum yields due to limited  $\pi$  conjugation of the formazanate framework. By comparison, the *p*-substituted analogs were slightly easier to reduce electrochemically, had dramatically red-shifted  $\lambda_{\text{max}}$  and  $\lambda_{\text{em}}$ , and significantly enhanced emission quantum yields (up to 0.77). Each of these traits were consistent with extended  $\pi$  conjugation between the formazanate backbone and the *N*-aryl substituents. The spectroscopic properties of the *m*-substituted complexes, which were the easiest to reduce, were intermediate between those of the *o*- and *p*- complexes, due to the absence of resonance delocalization of the oxygen lone pairs and the inductive electron withdrawing nature of the methoxy groups. Based on our evaluation, we were able to identify complex **7c** (Ar = *p*-anisole, R = cyano) as a strong candidate for use in fluorescence cell imaging applications. We subsequently demonstrated its efficacy as a fluorescent dye for orthogonal imaging of the cytoplasm (complex **7c**) and nucleus (DAPI) of mouse fibroblast cells. Our future work in this area will expand on these results and focus on cell imaging applications involving disease-targeting BF<sub>2</sub> formazanate dyes.

## Experimental Section

### General Considerations

All reactions were carried out under nitrogen atmosphere using standard Schlenk techniques unless otherwise stated. Reagents were purchased from Sigma-Aldrich or Alfa Aesar and used as received. Solvents were purchased from Caledon Laboratories, dried using an Innovative Technologies Inc. solvent purification system, collected under vacuum, and stored under inert (nitrogen) atmosphere containing 4 Å molecular sieves. The synthesis and characterization of compounds **4c** and **7c** have been reported previously.<sup>[13b]</sup> NMR spectra were recorded on 400 MHz (<sup>1</sup>H: 399.8 MHz, <sup>11</sup>B: 128.3 MHz, <sup>19</sup>F: 376.1 MHz) or 600 MHz (<sup>1</sup>H: 599.5 MHz, <sup>13</sup>C: 150.8 MHz) Varian INOVA spectrometers. <sup>1</sup>H NMR spectra were referenced to residual CHCl<sub>3</sub> (7.27 ppm) or (CD<sub>3</sub>)(CD<sub>2</sub>H)SO (2.50 ppm) and <sup>13</sup>C NMR spectra were referenced to CDCl<sub>3</sub> (77.0 ppm) or DMSO-*d*<sub>6</sub> (39.5 ppm). <sup>11</sup>B spectra were referenced to BF<sub>3</sub>·OEt<sub>2</sub> at 0 ppm, and <sup>19</sup>F spectra were referenced to CFC<sub>3</sub> at 0 ppm. Mass spectrometry data were recorded in positive-ion mode using a high-resolution Finnigan MAT 8200 spectrometer using electron impact ionization. UV-vis spectra were recorded using a Cary 300 Scan instrument. Molar extinction coefficients were determined from the slope of a plot of absorbance against concentration using four solutions with known concentrations ranging between 10 and 100 μM. Infrared spectra were recorded on a KBr disk using a Bruker Vector 33 FT-IR spectrometer. Emission spectra were obtained using a Photon Technology International QM-4 SE spectrofluorometer. Excitation wavelengths were chosen based on absorption maxima from the respective UV-vis spectrum in the same solvent. Quantum yields were calculated relative to ruthenium tris(bipyridine) hexafluorophosphate by methods described by Fery-Forgues and co-workers.<sup>[22]</sup>

### Electrochemical Methods

Cyclic voltammetry experiments were performed with a Bioanalytical

Systems Inc. (BASi) Epsilon potentiostat and analyzed using BASi Epsilon software. Typical electrochemical cells consisted of a three-electrode setup including a silver *pseudo* reference electrode, glassy carbon working electrode, and platinum counter electrode. Experiments were run at 100 mV s<sup>-1</sup> scan rate in degassed acetonitrile solutions of the analyte (~1 mM) and electrolyte (0.1 M tetrabutylammonium hexafluorophosphate). Cyclic voltammograms were referenced relative to the ferrocene/ferrocenium redox couple (~1 mM internal standard) and corrected for internal cell resistance using the BASi Epsilon software.

### X-ray Crystallography Methods

Single crystals of **7a** and **7b** were mounted on a Mitegen polyimide micromount with a small amount of Paratone N oil. X-ray diffraction measurements for **7a** were made on a Nonius KappaCCD Apex2 and measurements for **7b** were made using Bruker a Kappa Axis Apex2 diffractometer. Both compounds were measured at a temperature of 110 K. The data collection strategy was a number of  $\omega$  and  $\phi$  which collected data over a range of angles,  $2\theta$ . The frame integration was performed using SAINT.<sup>[23]</sup> The resulting raw data was scaled and absorption corrected using a multi-scan averaging of symmetry equivalent data using SADABS.<sup>[24]</sup>

The structures were solved by using a dual space methodology using the SHELXT program.<sup>[25]</sup> All non-hydrogen atoms were obtained from the initial solution. The hydrogen atoms were introduced at idealized positions and were allowed to refine isotropically. The structural model was fit to the data using full matrix least-squares based on  $F^2$ . The calculated structure factors included corrections for anomalous dispersion from the usual tabulation. The structures were refined using the SHELXL-2014 program from the SHELXTL program package.<sup>[26]</sup> See Table 4, the Supporting Information, and CCDC 1413166 and 1413167 for crystallographic details.

**Table 4.** X-ray diffraction data collection and refinement details for **7a** and **7b**.

	<b>7a</b>	<b>7b</b>
Chemical Formula	C <sub>16</sub> H <sub>14</sub> BF <sub>2</sub> N <sub>5</sub> O <sub>2</sub>	C <sub>16</sub> H <sub>14</sub> BF <sub>2</sub> N <sub>5</sub> O <sub>2</sub>
FW (g mol <sup>-1</sup> )	357.13	357.13
Crystal Dimensions (mm)	0.411 × 0.149 × 0.104	0.384 × 0.324 × 0.246
Crystal Habit	red needle	purple prism
Crystal System	monoclinic	monoclinic
Space Group	P2 <sub>1</sub> /c	C2/m
Temperature (K)	110	110
a (Å)	9.784(2)	13.349(3)
b (Å)	18.259(5)	16.206(3)
c (Å)	10.150(2)	8.1753(19)
α (°)	90	90
β (°)	111.382(6)	112.872(10)
γ (°)	90	90
V (Å <sup>3</sup> )	1688.4(7)	1629.6(6)
Z	4	4
ρ (g cm <sup>-3</sup> )	1.405	1.456
λ, Å	1.54178 (CuKα)	0.71073 (MoKα)
μ (cm <sup>-1</sup> )	0.938	0.114
Diffractometer Type	Nonius KappaCCD	Bruker Kappa Axis
R <sub>merge</sub>	Apex2 0.0380	Apex2 0.0272
R <sub>1</sub> [I > 2σ(I)]	0.0305	0.0387
ωR <sub>2</sub> [I > 2σ(I)]	0.0731	0.1127
R <sub>1</sub> (all data)	0.0376	0.0509
ωR <sub>2</sub> (all data)	0.0768	0.1210
GOF	1.054	1.058

$$R_1 = \frac{\sum(|F_o| - |F_c|)}{\sum F_o}; \omega R_2 = \frac{[\sum(\omega(F_o^2 - F_c^2)^2) / \sum(\omega F_o^4)]^{1/2}}{[\sum(\omega(F_o^2 - F_c^2)^2) / (\text{No. of reflns.} - \text{No. of params.})]^{1/2}}; \text{GOF} = \frac{[\sum(\omega(F_o^2 - F_c^2)^2) / (\text{No. of reflns.} - \text{No. of params.})]^{1/2}}{[\sum(\omega F_o^4)]^{1/2}}$$

### Cell Imaging Protocols

A stock solution of BF<sub>2</sub> formazanate complex **7c** in DMSO (10 μM) was prepared and subsequently diluted with Dulbecco's modified Eagle's

medium (DMEM) to obtain final concentrations of 0.5  $\mu\text{M}$  of dye. Mouse fibroblast C3H/10T1/2 cells (ATCC, Manassas, VA) were released from the tissue culture flask by trypsinization and seeded onto cover slips in a 12-well tissue culture plate at an approximate cell density of 50,000 cells per well. The cells were incubated overnight in DMEM containing 10% fetal bovine serum (FBS) at 37  $^{\circ}\text{C}$  in a 5%  $\text{CO}_2$  atmosphere. The serum containing DMEM in each well was removed and replaced with serum free DMEM containing a concentration of 0.5  $\mu\text{M}$  of dye and incubated at 37  $^{\circ}\text{C}$  for 1 h. The cells were then washed three times with phosphate buffer saline (PBS), fixed with 4% paraformaldehyde and mounted onto slides containing Pro-Long Antifade mounting medium with DAPI. Images were then obtained using an Olympus FluoView FV 1000 confocal microscope.

#### Representative Procedure for the Preparation of Formazans 4a, 4b, and 4d

**Formazan 4a ( $\text{Ar}_1 = \text{Ar}_5 = o\text{-anisole}$ ,  $\text{R}_3 = \text{CN}$ ).** In air, cyanoacetic acid (2.40 g, 28.2 mmol) and sodium hydroxide (11.4 g, 285 mmol) were dissolved in deionized water (140 mL). The resulting colorless solution was cooled to 0  $^{\circ}\text{C}$  and stirred for 2 h. In a separate flask, *o*-anisidine (6.92 g, 56.2 mmol) was combined with concentrated hydrochloric acid (14.0 mL, 168 mmol) in deionized water (55 mL) and stirred for 1.5 h at 0  $^{\circ}\text{C}$ . A solution of sodium nitrite (5.83 g, 84.5 mmol) in deionized water (17 mL) was cooled to 0  $^{\circ}\text{C}$  in an ice bath for 1.5 h before it was added dropwise to the *o*-anisidine solution over a 25 min period. The resulting yellow-brown diazonium salt solution was stirred for 1 h at 0  $^{\circ}\text{C}$  before it was added to the alkaline cyanoacetic acid solution. Upon addition, the solution turned blood red and a precipitate of the same color formed. The mixture was left to warm slowly with stirring for 18 h before the solid was isolated by vacuum filtration. The filtrate was neutralized with 1 M HCl (ca. 150 mL), extracted into dichloromethane (3  $\times$  150 mL), washed with deionized water (3  $\times$  150 mL), dried over  $\text{MgSO}_4$ , gravity filtered, and concentrated *in vacuo* to afford a red solid. The crude solids were combined and purified by flash column chromatography (dichloromethane, neutral alumina) and recrystallized from a saturated methanolic solution to afford formazan 4a as red needles. Yield = 6.10 g, 70%. M.p. 136–138  $^{\circ}\text{C}$ .  $^1\text{H}$  NMR (599.5 MHz,  $\text{CDCl}_3$ ):  $\delta$  13.91 (s, 1H, NH), 7.78 (d,  $^3J_{\text{HH}} = 8$  Hz, 2H, aryl CH), 7.34–7.31 (m, 2H, aryl CH), 7.06–7.02 (m, 4H, aryl CH), 7.19–7.17 (m, 2H, aryl CH), 6.92 (dd,  $^3J_{\text{HH}} = 8$  Hz,  $^4J_{\text{HH}} = 3$  Hz, 2H, aryl CH), 3.89 (s, 6H,  $\text{OCH}_3$ ); Linear Isomer (minor, 25%)  $\delta$  9.14 (s, 1H, NH), 7.53 (d,  $^3J_{\text{HH}} = 8$  Hz, 1H, aryl CH), 7.43–7.40 (m, 3H, aryl CH), 7.33–7.30 (m, 1H, aryl CH), 7.07–7.06 (m, 1H, aryl CH), 7.02 (m, 1H, aryl CH), 6.74–6.73 (m, 1H, aryl CH), 3.89 (s, 3H,  $\text{OCH}_3$ ), 3.88 (s, 3H,  $\text{OCH}_3$ ).  $^{13}\text{C}\{^1\text{H}\}$  NMR (150.8 MHz,  $\text{CDCl}_3$ ):  $\delta$  161.0, 160.8, 160.4, 153.2, 147.5, 142.0, 130.5, 130.3, 130.3, 129.9, 125.1, 119.2, 117.7, 115.7, 114.4, 113.0, 111.2, 108.0, 107.9, 105.6, 103.5, 100.9, 55.6 (br). FTIR (KBr): 3276 (m), 3086 (m), 3008 (m), 2960 (m), 2839 (m), 2227 (s), 1609 (s), 1535 (s), 1496 (s), 1412 (m), 1240 (s), 1150 (m), 1044 (s)  $\text{cm}^{-1}$ . UV-vis (toluene):  $\lambda_{\text{max}}$  432 nm ( $\epsilon = 20,150 \text{ M}^{-1} \text{ cm}^{-1}$ ). MS (EI = +ve mode): exact mass calculated for  $[\text{C}_{16}\text{H}_{15}\text{N}_5\text{O}_2]^+$ : 309.1226; exact mass found: 309.1221; difference: -1.6 ppm.

**Formazan 4b ( $\text{Ar}_1 = \text{Ar}_5 = m\text{-anisole}$ ,  $\text{R}_3 = \text{CN}$ ).** From 3.41 g (27.7 mmol) of *m*-anisidine. Yield = 0.751 g, 18% of a dark red microcrystalline solid. M.p. 132–134  $^{\circ}\text{C}$ .  $^1\text{H}$  NMR (599.5 MHz,  $\text{CDCl}_3$ ): Open Isomer (major, 75%)  $\delta$  12.89 (s, 1H, NH), 7.37 (t,  $^3J_{\text{HH}} = 8$  Hz, 2H, aryl CH), 7.22–7.21 (m, 2H, aryl CH), 7.19–7.17 (m, 2H, aryl CH), 6.92 (dd,  $^3J_{\text{HH}} = 8$  Hz,  $^4J_{\text{HH}} = 3$  Hz, 2H, aryl CH), 3.89 (s, 6H,  $\text{OCH}_3$ ); Linear Isomer (minor, 25%)  $\delta$  9.14 (s, 1H, NH), 7.53 (d,  $^3J_{\text{HH}} = 8$  Hz, 1H, aryl CH), 7.43–7.40 (m, 3H, aryl CH), 7.33–7.30 (m, 1H, aryl CH), 7.07–7.06 (m, 1H, aryl CH), 7.02 (m, 1H, aryl CH), 6.74–6.73 (m, 1H, aryl CH), 3.89 (s, 3H,  $\text{OCH}_3$ ), 3.88 (s, 3H,  $\text{OCH}_3$ ).  $^{13}\text{C}\{^1\text{H}\}$  NMR (150.8 MHz,  $\text{CDCl}_3$ ):  $\delta$  161.0, 160.8, 160.4, 153.2, 147.5, 142.0, 130.5, 130.3, 130.3, 129.9, 125.1, 119.2, 117.7, 115.7, 114.4, 113.0, 111.2, 108.0, 107.9, 105.6, 103.5, 100.9, 55.6 (br). FTIR (KBr): 3276 (m), 3086 (m), 3008 (m), 2960 (m), 2839 (m), 2227 (s), 1609 (s), 1535 (s), 1496 (s), 1412 (m), 1240 (s), 1150 (m), 1044 (s)  $\text{cm}^{-1}$ . UV-vis (toluene):  $\lambda_{\text{max}}$  432 nm ( $\epsilon = 20,150 \text{ M}^{-1} \text{ cm}^{-1}$ ). MS (EI = +ve mode): exact mass calculated for  $[\text{C}_{16}\text{H}_{15}\text{N}_5\text{O}_2]^+$ : 309.1226; exact mass found: 309.1221; difference: -1.6 ppm.

**Formazan 4d ( $\text{Ar}_1 = \text{Ar}_5 = o\text{-ethylbenzene}$ ,  $\text{R}_3 = \text{CN}$ ).** From 2.96 g (24.4 mmol) of 2-ethylaniline. Yield = 0.322 g, 9% of a dark red powder. M.p. 89–91  $^{\circ}\text{C}$ .  $^1\text{H}$  NMR (599.5 MHz,  $\text{CDCl}_3$ ): Open Isomer (major, 81%)  $\delta$  11.75 (s, 1H, NH), 7.67–7.65 (m, 2H, aryl CH), 7.34–7.31 (m, 6H, aryl CH), 2.97 (q,  $^3J_{\text{HH}} = 8$  Hz, 4H,  $\text{CH}_2\text{CH}_3$ ), 1.35 (m, 6H,  $\text{CH}_2\text{CH}_3$ ); Linear Isomer (minor, 29%)  $\delta$  9.17 (s, 1H, NH), 7.77 (d,  $^3J_{\text{HH}} = 8$  Hz, 1H, aryl CH), 7.72 (m, 1H, aryl CH), 7.44 (m, 2H, aryl CH), 7.40 (m, 2H, aryl CH), 7.30–7.28 (m, 1H, aryl CH), 7.15 (m, 1H, CH), 3.18 (q,  $^3J_{\text{HH}} = 8$  Hz, 4H,  $\text{CH}_2\text{CH}_3$ ), 2.80 (q,  $^3J_{\text{HH}} = 8$  Hz, 2H,  $\text{CH}_2\text{CH}_3$ ), 1.39 (m, 6H,  $\text{CH}_2\text{CH}_3$ ).  $^{13}\text{C}\{^1\text{H}\}$  NMR (150.8 MHz,  $\text{CDCl}_3$ ):  $\delta$  149.3, 145.3, 144.2, 138.1, 137.8, 132.3, 131.9, 130.0, 129.6, 129.5, 129.1, 129.0, 127.6, 127.4, 127.2, 126.5, 124.8, 115.6, 115.5, 115.4, 113.3, 108.0, 24.7, 24.2, 23.5, 16.3, 15.0, 13.8. FTIR (KBr): 3338 (m), 3077 (m), 2973 (m), 2936 (m), 2878 (m), 2227 (m), 1589 (m), 1529 (s), 1457 (m), 1276 (m), 1201 (m), 1157 (m), 1060 (w)  $\text{cm}^{-1}$ . UV-vis (toluene):  $\lambda_{\text{max}}$  419 nm ( $\epsilon = 25,500 \text{ M}^{-1} \text{ cm}^{-1}$ ). MS (EI = +ve mode): exact mass calculated for  $[\text{C}_{18}\text{H}_{19}\text{N}_5]^+$ : 305.1640; exact mass found: 305.1639; difference: -0.3 ppm.

#### Representative Procedure for the Preparation of Formazans 5a and 5b

**Formazan 5a ( $\text{Ar}_1 = \text{Ar}_5 = o\text{-anisole}$ ,  $\text{R}_3 = \text{NO}_2$ ).** The following procedure was adapted from a protocol developed by von Eschwege and co-workers.<sup>[19b]</sup> In air, *o*-anisidine (3.63 g, 29.5 mmol) was added to deionized water (28 mL) containing concentrated hydrochloric acid (16.0 mL, 192 mmol). The mixture was cooled to -10  $^{\circ}\text{C}$  in an acetone/ice bath and stirred for 1 h. In a separate flask, sodium nitrite (3.22 g, 46.7 mmol) was dissolved in deionized water (9.20 mL) and cooled to -10  $^{\circ}\text{C}$  in an acetone/ice bath for 30 min. The sodium nitrite solution was added to the *o*-anisidine mixture dropwise over the course of 30 min. The resulting yellow-brown diazonium salt solution was then added to a flask containing sodium acetate (28.5 g, 347 mmol), glacial acetic acid (29.0 mL) and deionized water (14 mL) and stirred at room temperature for 5 min. Nitromethane (8.98 g, 7.97 mL, 147 mmol) was then added and the solution was stirred for 1 h before deionized water (1.60 L) was added. The solution was stirred for an additional 30 min and vacuum filtered to afford a red solid. The filtrate was extracted into dichloromethane (3  $\times$  250 mL), washed with deionized water (4  $\times$  200 mL), dried over  $\text{MgSO}_4$ , gravity filtered and concentrated *in vacuo* to afford a dark red solid. The crude solids were combined and purified by flash column chromatography (dichloromethane, neutral alumina) to afford formazan 5a as a dark red microcrystalline solid. Yield = 4.01 g, 82%. M.p. 176–178  $^{\circ}\text{C}$ .  $^1\text{H}$  NMR (599.5 MHz,  $\text{CDCl}_3$ ):  $\delta$  14.87 (s, 1H, NH), 7.97–7.95 (m, 2H, aryl CH), 7.38–7.35 (m, 2H, aryl CH), 7.08–7.05 (m, 2H, aryl CH), 7.04–7.03 (m, 2H, aryl CH), 4.02 (s, 6H,  $\text{OCH}_3$ ).  $^{13}\text{C}\{^1\text{H}\}$  NMR (150.8 MHz,  $\text{CDCl}_3$ ):  $\delta$  153.0, 136.2, 130.8, 121.6, 117.0, 112.0, 56.1. FTIR (KBr): 3057 (m), 2990 (m), 1660 (m), 1578 (s), 1423 (m), 1267 (m), 897 (m)  $\text{cm}^{-1}$ . UV-vis (toluene):  $\lambda_{\text{max}}$  472 nm ( $\epsilon = 8,000 \text{ M}^{-1} \text{ cm}^{-1}$ ). MS (EI = +ve mode): exact mass calculated for  $[\text{C}_{15}\text{H}_{15}\text{N}_5\text{O}_4]^+$ : 329.1124; exact mass found: 329.1121; difference: -0.9 ppm.

**Formazan 5b ( $\text{Ar}_1 = \text{Ar}_5 = m\text{-anisole}$ ,  $\text{R}_3 = \text{NO}_2$ ).** From 2.19 g (17.8 mmol) of *m*-anisidine. Yield = 1.77 g, 60% of dark red microcrystalline solid. M.p. 134–136  $^{\circ}\text{C}$ .  $^1\text{H}$  NMR (599.5 MHz,  $\text{CDCl}_3$ ):  $\delta$  15.08 (s, 1H, NH), 7.35 (t,  $^3J_{\text{HH}} = 8$  Hz, 2H, aryl CH), 7.24–7.23 (m, 2H, aryl CH), 7.21–7.19 (m, 2H, aryl CH), 6.92 (dd,  $^3J_{\text{HH}} = 8$  Hz,  $^4J_{\text{HH}} = 2$  Hz, 2H, aryl CH), 3.85 (s, 6H,  $\text{OCH}_3$ ).  $^{13}\text{C}\{^1\text{H}\}$  NMR (150.8 MHz,  $\text{CDCl}_3$ ):  $\delta$  160.8, 147.2, 130.3, 116.4, 113.8, 103.3, 55.5. FTIR (KBr): 3058 (m), 3018 (m), 2973 (m), 2858 (m), 1661 (m), 1610 (s), 1552 (m), 1493 (w), 1434 (w), 1360 (w), 1267 (s), 1143 (w), 1045 (w), 896 (w), 826 (s)  $\text{cm}^{-1}$ . UV-vis (toluene):  $\lambda_{\text{max}}$  466 nm ( $\epsilon = 21,200 \text{ M}^{-1} \text{ cm}^{-1}$ ). MS (EI = +ve mode): exact mass calculated for  $[\text{C}_{15}\text{H}_{15}\text{N}_5\text{O}_4]^+$ : 329.1124; exact mass found: 329.1118; difference: -1.8 ppm.

**Preparation of Formazan 5c** ( $\text{Ar}_1 = \text{Ar}_5 = p\text{-anisole}$ ,  $\text{R}_3 = \text{NO}_2$ ). In air, nitromethane (1.23 g, 1.08 mL, 20.0 mmol) was combined with deionized water (150 mL), and sodium hydroxide (1.76 g, 44.0 mmol) before the mixture was cooled to 0 °C in an ice bath. In a separate flask, *p*-anisidine (5.00 g, 41.0 mmol) and concentrated hydrochloric acid (11.1 mL, 133 mmol) were mixed with deionized water (15 mL) and cooled to 0 °C in an ice bath. A cooled solution (0 °C) of sodium nitrite (3.35 g, 49.0 mmol) in deionized water (10 mL) was added slowly to the amine solution. This mixture was left to stir at 0 °C for 30 min, at which time the dark yellow diazonium salt solution was added dropwise to the nitromethane solution described above over a 10 min period. The resulting mixture was left to warm slowly with stirring for 18 h, during which time a dark red precipitate had formed. The dark red solid was isolated by vacuum filtration and purified by flash column chromatography (dichloromethane, neutral alumina) to afford formazan **5c** as a dark red microcrystalline solid. Yield = 6.59 g, 55%. M.p. 162–164 °C.  $^1\text{H}$  NMR (599.5 MHz,  $\text{DMSO}-d_6$ ):  $\delta$  14.61 (s, 1H, NH), 7.86 (d,  $^3J_{\text{HH}} = 8$  Hz, 4H, aryl CH), 7.11 (d,  $^3J_{\text{HH}} = 8$  Hz, 4H, aryl CH), 3.85 (s, 6H, OCH<sub>3</sub>).  $^{13}\text{C}\{^1\text{H}\}$  NMR (150.8 MHz,  $\text{DMSO}-d_6$ ):  $\delta$  160.5, 140.1, 121.8, 114.9, 55.7. FTIR (KBr): 3061 (m), 3018 (m), 2995 (m), 1659 (m), 1574 (w), 1428 (m), 1348 (w), 1268 (s), 1159 (w), 899 (m), 745 (m)  $\text{cm}^{-1}$ . UV-vis (toluene):  $\lambda_{\text{max}}$  504 nm ( $\epsilon = 18,400 \text{ M}^{-1} \text{ cm}^{-1}$ ). MS (EI, +ve mode): exact mass calculated for  $[\text{C}_{15}\text{H}_{15}\text{N}_5\text{O}_4]^+$ : 329.1124; exact mass found: 329.1123; difference: -0.3 ppm.

#### Representative Procedure for Preparation of Formazans 6a–c

**Formazan 6a** ( $\text{Ar}_1 = \text{Ar}_5 = o\text{-anisole}$ ,  $\text{R}_3 = \text{Ph}$ ). In air, phenylpyruvic acid (1.0 g, 6.1 mmol) and sodium hydroxide (1.83 g, 45.7 mmol) were combined with deionized water (150 mL) and cooled to 0 °C in an ice bath for 30 min. In a separate flask, *o*-anisidine (1.50 g, 12.2 mmol) and concentrated hydrochloric acid (3.5 mL, 42 mmol) were mixed in deionized water (10 mL), and cooled to 0 °C in an ice bath for 10 min. A cooled solution (0 °C) of sodium nitrite (0.97 g, 14.0 mmol) in deionized water (5 mL) was added slowly to the amine solution over a 10 min period. This yellow mixture was left to stir at 0 °C for 30 min, at which time it was added dropwise to the phenylpyruvic acid reaction mixture described above over a 10 min period. The resulting solution was left to warm slowly with stirring for 18 h, at which time a purple precipitate had formed. The purple solid was isolated by filtration and purified by flash column chromatography (dichloromethane, neutral alumina) to afford formazan **6a** as a purple microcrystalline solid. Yield = 1.98 g, 90%. M.p. 120–122 °C.  $^1\text{H}$  NMR (599.5 MHz,  $\text{CDCl}_3$ ):  $\delta$  15.01 (s, 1H, NH), 8.24–8.23 (m, 2H, aryl CH), 7.98–7.97 (m, 2H, aryl CH), 7.49–7.46 (m, 2H, aryl CH), 7.38–7.36 (m, 1H, aryl CH), 7.28–7.25 (m, 2H, aryl CH), 7.10–7.07 (m, 2H, aryl CH), 7.04–7.02 (m, 2H, aryl CH), 4.02 (s, 6H, OCH<sub>3</sub>).  $^{13}\text{C}\{^1\text{H}\}$  NMR (100.6 MHz,  $\text{CDCl}_3$ ):  $\delta$  152.0, 142.2, 138.0, 137.9, 128.3, 128.0, 127.3, 125.8, 121.3, 115.7, 111.7, 56.0. FT-IR (KBr): 3076 (m), 3008 (m), 2915 (m), 1659 (m), 1267 (m), 1106 (s), 752 (m)  $\text{cm}^{-1}$ . UV-vis (toluene):  $\lambda_{\text{max}}$  = 507 nm ( $\epsilon = 22,900 \text{ M}^{-1} \text{ cm}^{-1}$ ). Mass Spec. (EI, +ve mode): exact mass calculated for  $[\text{C}_{21}\text{H}_{20}\text{N}_4\text{O}_2]^+$ : 360.1586; exact mass found: 360.1580; difference: -1.7 ppm.

**Formazan 6b** ( $\text{Ar}_1 = \text{Ar}_5 = m\text{-anisole}$ ,  $\text{R}_3 = \text{Ph}$ ). From 1.50 g (12.2 mmol) of *m*-anisidine. Yield = 1.38 g, 63% as a dark red solid. M.p. 99–101 °C.  $^1\text{H}$  NMR (599.5 MHz,  $\text{CDCl}_3$ ):  $\delta$  15.35 (s, 1H, NH), 8.15–8.14 (m, 2H, aryl CH), 7.48–7.46 (m, 2H, aryl CH), 7.39–7.36 (m, 3H, aryl CH), 7.31 (s, 2H, aryl CH), 7.24–7.23 (m, 2H, aryl CH), 6.87–6.85 (m, 2H, aryl CH), 3.91 (s, 6H, OCH<sub>3</sub>).  $^{13}\text{C}\{^1\text{H}\}$  NMR (100.6 MHz,  $\text{CDCl}_3$ ):  $\delta$  160.7, 149.1, 141.0, 137.3, 130.0, 128.4, 127.6, 125.8, 113.4, 112.6, 102.9, 55.4. FTIR (KBr): 3057 (m), 2991 (m), 1660 (m), 1643 (m), 1426 (m), 1268 (s), 1103 (s), 898 (m), 745 (m)  $\text{cm}^{-1}$ . UV-vis (toluene):  $\lambda_{\text{max}}$  = 496 nm ( $\epsilon = 21,600 \text{ M}^{-1} \text{ cm}^{-1}$ ). Mass Spec. (EI, +ve mode): exact mass calculated for  $[\text{C}_{21}\text{H}_{20}\text{N}_4\text{O}_2]^+$ : 360.1586; exact mass found: 360.1584; difference: -0.6 ppm.

**Formazan 6c** ( $\text{Ar}_1 = \text{Ar}_5 = p\text{-anisole}$ ,  $\text{R}_3 = \text{Ph}$ ). From 1.48 g (12.0 mmol) of *p*-anisidine. Yield = 1.69 g, 82% as a dark red solid. M.p. 122–124 °C.  $^1\text{H}$  NMR (599.5 MHz,  $\text{CDCl}_3$ ):  $\delta$  15.56 (s, 1H, NH), 8.13 (d,  $^3J_{\text{HH}} = 7$  Hz, 2H, aryl CH), 7.65 (d,  $^3J_{\text{HH}} = 9$  Hz, 4H, aryl CH), 7.45–7.43 (m, 2H, aryl CH), 7.34 (t,  $^3J_{\text{HH}} = 8$  Hz, 1H, aryl CH), 6.99 (d,  $^3J_{\text{HH}} = 9$  Hz, 4H, aryl CH), 3.88 (s, 6H, OCH<sub>3</sub>).  $^{13}\text{C}\{^1\text{H}\}$  NMR (100.6 MHz,  $\text{CDCl}_3$ ):  $\delta$  159.2, 142.0, 140.6, 137.8, 128.3, 127.2, 125.6, 120.0, 114.7, 55.6. FTIR (KBr): 3263 (br, s), 2984 (m), 2884 (w), 2794 (s), 1594 (s), 1573 (m), 1507 (s), 1495 (s), 1226 (s), 1176 (m)  $\text{cm}^{-1}$ . UV-vis (toluene):  $\lambda_{\text{max}}$  = 530 nm ( $\epsilon = 23,400 \text{ M}^{-1} \text{ cm}^{-1}$ ). Mass Spec. (EI, +ve mode): exact mass calculated for  $[\text{C}_{21}\text{H}_{20}\text{N}_4\text{O}_2]^+$ : 360.1586; exact mass found: 360.1581; difference: -1.4 ppm.

#### Representative Procedure for the Preparation of Formazanate BF<sub>2</sub> Complexes 7a and 7d.

**Formazanate BF<sub>2</sub> Complex 7a** ( $\text{Ar}_1 = \text{Ar}_5 = o\text{-anisole}$ ,  $\text{R}_3 = \text{CN}$ ). Formazan **4a** (0.500 g, 1.61 mmol) was dissolved in toluene (250 mL) before triethylamine (1.45 g, 2.00 mL, 14.2 mmol) was added and the solution stirred for 30 min. Boron trifluoride diethyl etherate (3.45 g, 3.00 mL, 24.3 mmol) was then added and the solution heated to 105 °C for 36 h. During this time, the solution gradually changed color from dark red to red-orange. The solution was cooled to 20 °C and deionized water (25 mL) was added to quench any remaining reactive species. The mixture was then washed with deionized water (3 × 50 mL), dried over  $\text{MgSO}_4$ , gravity filtered, and concentrated *in vacuo* to afford **7a** as a red-orange solid. The crude solid was purified via flash column chromatography (dichloromethane, neutral alumina) to afford **7a** as a bright orange powder. This compound hydrolyzes slowly. Analyses were performed using dry solvents. Yield = 0.353 g, 61%. M.p. 134–136 °C.  $^1\text{H}$  NMR (599.5 MHz, *dry*  $\text{CDCl}_3$ ):  $\delta$  7.46–7.43 (m, 2H, aryl CH), 7.30–7.28 (m, 2H, aryl CH), 7.05–7.01 (m, 4H, aryl CH), 3.91 (s, 6H, OCH<sub>3</sub>).  $^{13}\text{C}\{^1\text{H}\}$  NMR (150.8 MHz,  $\text{CDCl}_3$ ):  $\delta$  154.8, 132.5, 132.4, 127.2, 120.8, 113.8, 112.8, 56.4.  $^{11}\text{B}$  NMR (128.3 MHz,  $\text{CDCl}_3$ ):  $\delta$  -1.9 (t,  $^1J_{\text{BF}} = 20$  Hz).  $^{19}\text{F}$  NMR (376.1 MHz,  $\text{CDCl}_3$ ):  $\delta$  -154.3 (q,  $^1J_{\text{FB}} = 19$  Hz). FTIR (KBr): 3072 (m), 3017 (m), 2960 (m), 2853 (m), 2237 (s), 1605 (s), 1488 (s), 1340 (s), 1260 (s), 1195 (s), 1164 (s), 1030 (s)  $\text{cm}^{-1}$ . UV-vis (toluene):  $\lambda_{\text{max}}$  467 nm ( $\epsilon = 16,000 \text{ M}^{-1} \text{ cm}^{-1}$ ). MS (EI +ve mode): exact mass calculated for  $[\text{C}_{16}\text{H}_{14}\text{BF}_2\text{N}_5\text{O}_2]^+$ : 357.1209; exact mass found: 357.1212; difference: +0.8 ppm.

**Formazanate BF<sub>2</sub> Complex 7d** ( $\text{Ar}_1 = \text{Ar}_5 = o\text{-ethylbenzene}$ ,  $\text{R}_3 = \text{CN}$ ). From 0.366 g (1.20 mmol) of formazan **4d**. Yield = 0.095 g, 22% of dark orange oil.  $^1\text{H}$  NMR (599.5 MHz,  $\text{CDCl}_3$ ):  $\delta$  7.47–7.45 (m, 2H, aryl CH), 7.42–7.39 (m, 4H, aryl CH), 7.34–7.31 (m, 2H, aryl CH), 2.65 (q,  $^3J_{\text{HH}} = 8$  Hz, 4H, CH<sub>2</sub>CH<sub>3</sub>), 1.24 (t,  $^3J_{\text{HH}} = 7$  Hz, 6H, CH<sub>2</sub>CH<sub>3</sub>).  $^{13}\text{C}\{^1\text{H}\}$  NMR (150.8 MHz,  $\text{CDCl}_3$ ):  $\delta$  140.9, 139.7, 131.0, 130.5, 126.6, 126.3, 113.4, 24.3, 14.9.  $^{11}\text{B}$  NMR (128.3 MHz,  $\text{CDCl}_3$ ):  $\delta$  -1.9 (t,  $^1J_{\text{BF}} = 24$  Hz).  $^{19}\text{F}$  (376.1 MHz,  $\text{CDCl}_3$ ):  $\delta$  -146.9 (q,  $^1J_{\text{FB}} = 24$  Hz). FTIR (KBr): 3077 (m), 2975 (s), 2938 (s), 2879 (m), 2247 (m), 1453 (s), 1336 (s), 1217 (s), 1084 (s), 1025 (s), 970 (s)  $\text{cm}^{-1}$ . UV-vis (toluene):  $\lambda_{\text{max}}$  436 nm ( $\epsilon = 14,000 \text{ M}^{-1} \text{ cm}^{-1}$ ). MS (EI +ve mode): exact mass calculated for  $[\text{C}_{18}\text{H}_{18}\text{BF}_2\text{N}_5]^+$ : 353.1623; exact mass found: 353.1626; difference: +0.8 ppm.

#### Representative Procedure for the Preparation of Formazanate BF<sub>2</sub> Complexes 7b, 8b,c, and 9a–c

**Formazanate BF<sub>2</sub> Complex 7b** ( $\text{Ar}_1 = \text{Ar}_5 = m\text{-anisole}$ ,  $\text{R}_3 = \text{CN}$ ). Formazan **4b** (0.398 g, 1.28 mmol) was dissolved in toluene (175 mL) before triethylamine (0.391 g, 0.540 mL, 3.86 mmol) was added and the solution stirred for 30 min. Boron trifluoride diethyl etherate (0.92 g, 0.80 mL, 6.5 mmol) was then added and the solution heated to 80 °C for 18 h. During this time, the solution gradually changed color from dark red to purple. The solution was cooled to 20 °C and deionized water (15 mL) was added to quench any remaining reactive species. The mixture was

then washed with deionized water (3 × 50 mL), dried over MgSO<sub>4</sub>, gravity filtered, and concentrated *in vacuo* to afford **7b** as a purple solid. The crude solid was purified via flash column chromatography (dichloromethane, neutral alumina) and recrystallized from a saturated methanolic solution to afford **7b** as a purple microcrystalline solid. Yield = 0.221 g, 48%. M.p. 143–145 °C. <sup>1</sup>H NMR (599.5 MHz, CDCl<sub>3</sub>): δ 7.55 (d, <sup>3</sup>J<sub>HH</sub> = 9 Hz, 2H, aryl C<sub>H</sub>), 7.42–7.40 (m, 4H, aryl C<sub>H</sub>), 7.08 (dd, <sup>3</sup>J<sub>HH</sub> = 8 Hz, <sup>4</sup>J<sub>HH</sub> = 3 Hz, 2H, aryl C<sub>H</sub>), 3.89 (s, 6H, OC<sub>H</sub><sub>3</sub>). <sup>13</sup>C{<sup>1</sup>H} NMR (150.8 MHz, CDCl<sub>3</sub>): δ 160.4, 144.1, 130.2, 118.2, 116.0 (t, <sup>4</sup>J<sub>CF</sub> = 3 Hz), 114.0, 107.6, 55.7. <sup>11</sup>B NMR (128.3 MHz, CDCl<sub>3</sub>): δ -0.8 (t, <sup>1</sup>J<sub>BF</sub> = 31 Hz). <sup>19</sup>F (376.1 MHz, CDCl<sub>3</sub>): δ -132.6 (q, <sup>1</sup>J<sub>FB</sub> = 29 Hz). FTIR (KBr): 3072 (m), 3016 (m), 2958 (m), 2850 (m), 2237 (s), 1605 (s), 1582 (s), 1487 (s), 1456 (m), 1339 (s), 1293 (m), 1260 (s), 1195 (m), 1164 (m), 1031 (s) cm<sup>-1</sup>. UV-vis (toluene): λ<sub>max</sub> 525 nm (ε = 21,100 M<sup>-1</sup> cm<sup>-1</sup>). MS (EI, +ve mode): exact mass calculated for [C<sub>16</sub>H<sub>14</sub>BF<sub>2</sub>N<sub>5</sub>O<sub>2</sub>]<sup>+</sup>: 357.1209; exact mass found: 357.1198; difference: -3.1 ppm.

**Formazanate BF<sub>2</sub> Complex 8b (Ar<sub>1</sub> = Ar<sub>5</sub> = *m*-anisole, R<sub>3</sub> = NO<sub>2</sub>).** From 0.398 g (1.21 mmol) of formazan **5b**. Yield = 0.111 g, 24% of dark purple microcrystalline solid. M.p. 78–80 °C. <sup>1</sup>H NMR (599.5 MHz, CDCl<sub>3</sub>): δ 7.64–7.62 (m, 2H, aryl C<sub>H</sub>), 7.52–7.50 (m, 2H, aryl C<sub>H</sub>), 7.43 (t, <sup>3</sup>J<sub>HH</sub> = 8 Hz, 2H, aryl C<sub>H</sub>), 7.09 (dd, <sup>3</sup>J<sub>HH</sub> = 8 Hz, <sup>4</sup>J<sub>HH</sub> = 2 Hz, 2H, aryl C<sub>H</sub>), 3.90 (s, 6H, OC<sub>H</sub><sub>3</sub>). <sup>13</sup>C{<sup>1</sup>H} NMR (150.8 MHz, CDCl<sub>3</sub>): δ 160.5, 144.2, 130.3, 118.5, 116.3 (<sup>4</sup>J<sub>CF</sub> = 4 Hz), 108.0, 55.7. <sup>11</sup>B NMR (128.3 MHz, CDCl<sub>3</sub>): δ -0.7 (t, <sup>1</sup>J<sub>BF</sub> = 29 Hz). <sup>19</sup>F (376.1 MHz, CDCl<sub>3</sub>): δ -134.6 (q, <sup>1</sup>J<sub>FB</sub> = 29 Hz). FTIR (KBr): 3076 (m), 3013 (m), 2863 (m), 1658 (m), 1580 (m), 1424 (m), 1266 (m), 1095 (s), 745 (m) cm<sup>-1</sup>. UV-vis (toluene): λ<sub>max</sub> 533 nm (ε = 18,400 M<sup>-1</sup> cm<sup>-1</sup>). MS (EI, +ve mode): exact mass calculated for [C<sub>15</sub>H<sub>14</sub>BF<sub>2</sub>N<sub>5</sub>O<sub>4</sub>]<sup>+</sup>: 377.1107; exact mass found: 377.1104; difference: -0.8 ppm.

**Formazanate BF<sub>2</sub> Complex 8c (Ar<sub>1</sub> = Ar<sub>5</sub> = *p*-anisole, R<sub>3</sub> = NO<sub>2</sub>).** From 1.19 g (3.60 mmol) of formazan **5c**. Yield = 0.291 g, 21% of dark purple microcrystalline solid. M.p. 154–156 °C. <sup>1</sup>H NMR (599.5 MHz, CDCl<sub>3</sub>): δ 7.99 (d, <sup>3</sup>J<sub>HH</sub> = 9 Hz, 4H, aryl C<sub>H</sub>), 7.01 (dd, <sup>3</sup>J<sub>HH</sub> = 9 Hz, <sup>4</sup>J<sub>HH</sub> = 2 Hz, 4H, aryl C<sub>H</sub>), 3.91 (s, 6H, OC<sub>H</sub><sub>3</sub>). <sup>13</sup>C{<sup>1</sup>H} NMR (150.8 MHz, CDCl<sub>3</sub>): δ 162.4, 137.0, 125.2, 114.9, 100.0, 55.8. <sup>11</sup>B NMR (128.3 MHz, CDCl<sub>3</sub>): δ -0.7 (t, <sup>1</sup>J<sub>BF</sub> = 30 Hz). <sup>19</sup>F (376.1 MHz, CDCl<sub>3</sub>): δ -137.1 (q, <sup>1</sup>J<sub>FB</sub> = 29 Hz). FTIR (KBr): 3058 (m), 3011 (m), 2993 (m), 1656 (m), 1580 (w), 1420 (m), 1340 (w), 1270 (s), 1151 (w), 900 (m), 745 (m) cm<sup>-1</sup>. UV-vis (toluene): λ<sub>max</sub> 579 nm (ε = 23,600 M<sup>-1</sup> cm<sup>-1</sup>). MS (EI, +ve mode): exact mass calculated for [C<sub>15</sub>H<sub>14</sub>BF<sub>2</sub>N<sub>5</sub>O<sub>4</sub>]<sup>+</sup>: 377.1107; exact mass found: 377.1101; difference: -1.6 ppm.

**Formazanate BF<sub>2</sub> Complex 9a (Ar<sub>1</sub> = Ar<sub>5</sub> = *o*-anisole, R<sub>3</sub> = Ph).** This complex required additional purification by flash column chromatography (toluene, silica gel). From 0.396 g (1.10 mmol) of formazan **6a**. Yield = 0.212 g, 47% of an orange solid. M.p. 158–160 °C. <sup>1</sup>H NMR (399.5 MHz, CDCl<sub>3</sub>): δ 8.08–8.06 (m, 2H, aryl C<sub>H</sub>), 7.46–7.38 (m, 5H, aryl C<sub>H</sub>), 7.23–7.22 (m, 2H, aryl C<sub>H</sub>), 7.04–6.99 (m, 4H, aryl C<sub>H</sub>), 3.92 (s, 6H, OC<sub>H</sub><sub>3</sub>). <sup>13</sup>C{<sup>1</sup>H} NMR (100.6 MHz, CDCl<sub>3</sub>): δ 155.0, 151.5, 133.3, 133.1, 130.9, 129.2, 128.5, 127.3, 125.7, 120.6, 112.5, 56.3. <sup>11</sup>B NMR (128.3 MHz, CDCl<sub>3</sub>): δ -1.2 (t, <sup>1</sup>J<sub>BF</sub> = 19 Hz). <sup>19</sup>F NMR (376.1 MHz, CDCl<sub>3</sub>): δ -160.6 (q, <sup>1</sup>J<sub>FB</sub> = 19 Hz). FTIR (KBr): 3057 (m), 2988 (m), 2967 (w), 2843 (m), 1666 (m), 1496 (s), 1441 (m), 1359 (m), 1268 (s), 1124 (s), 1050 (m), 897 (m), 745 (m) cm<sup>-1</sup>. UV-vis (toluene): λ<sub>max</sub> 467 nm (ε = 18,800 M<sup>-1</sup> cm<sup>-1</sup>). Mass Spec. (EI, +ve mode): exact mass calculated for [C<sub>21</sub>H<sub>19</sub>BF<sub>2</sub>N<sub>4</sub>O<sub>2</sub>]<sup>+</sup>: 408.1569; exact mass found: 408.1564; difference: -1.2 ppm.

**Formazanate BF<sub>2</sub> Complex 9b (Ar<sub>1</sub> = Ar<sub>5</sub> = *m*-anisole, R<sub>3</sub> = Ph).** From 0.613 g (1.70 mmol) of formazan **6b**. Yield = 0.621 g, 90% of a purple-red solid. M.p. 76–78 °C. <sup>1</sup>H NMR (399.8 MHz, CDCl<sub>3</sub>): δ 8.14–8.13 (m, 2H, aryl C<sub>H</sub>), 7.57–7.56 (m, 2H, aryl C<sub>H</sub>), 7.52–7.49 (m, 2H, aryl C<sub>H</sub>), 7.47–7.46 (m, 3H, aryl C<sub>H</sub>), 7.41–7.39 (m, 2H, aryl C<sub>H</sub>), 7.02–7.01 (m,

2H, aryl C<sub>H</sub>), 3.89 (s, 6H, OC<sub>H</sub><sub>3</sub>). <sup>13</sup>C{<sup>1</sup>H} NMR (100.6 MHz, CDCl<sub>3</sub>): δ 160.1, 148.9, 145.0, 133.5, 129.8, 129.3, 128.7, 125.5, 116.1 (m), 116.0, 108.5, 55.5. <sup>11</sup>B NMR (128.3 MHz, CDCl<sub>3</sub>): δ -0.6 (t, <sup>1</sup>J<sub>BF</sub> = 29 Hz). <sup>19</sup>F NMR (376.1 MHz, CDCl<sub>3</sub>): δ -144.2 (q, <sup>1</sup>J<sub>FB</sub> = 28 Hz). FTIR (KBr): 3058 (m), 2989 (m), 2900 (m), 2841 (w), 1667 (m), 1605 (m), 1494 (m), 1424 (m), 1357 (w), 1267 (s), 1119 (m), 897 (w), 745 (m) cm<sup>-1</sup>. UV-vis (toluene): λ<sub>max</sub> 530 nm (ε = 22,900 M<sup>-1</sup> cm<sup>-1</sup>). Mass Spec. (EI, +ve mode): exact mass calculated for [C<sub>21</sub>H<sub>19</sub>BF<sub>2</sub>N<sub>4</sub>O<sub>2</sub>]<sup>+</sup>: 408.1569; exact mass found: 408.1570; difference: +0.2 ppm.

**Formazanate BF<sub>2</sub> Complex 9c (Ar<sub>1</sub> = Ar<sub>5</sub> = *p*-anisole, R<sub>3</sub> = Ph).** From 1.00 g (2.80 mmol) of formazan **6c**. Yield = 0.711 g, 62% of a dark purple solid. M.p. 170–172 °C. <sup>1</sup>H NMR (399.8 MHz, CDCl<sub>3</sub>): δ 8.12 (d, <sup>3</sup>J<sub>HH</sub> = 7 Hz, 2H, aryl C<sub>H</sub>), 7.88 (d, <sup>3</sup>J<sub>HH</sub> = 9 Hz, 4H, aryl C<sub>H</sub>), 7.49–7.41 (m, 3H, aryl C<sub>H</sub>), 6.98 (d, <sup>3</sup>J<sub>HH</sub> = 9 Hz, 4H, aryl C<sub>H</sub>), 3.88 (s, 6H, OC<sub>H</sub><sub>3</sub>). <sup>13</sup>C{<sup>1</sup>H} NMR (100.6 MHz, CDCl<sub>3</sub>): δ 160.7, 137.6, 134.0, 128.9, 128.6, 125.4, 124.9, 114.3, 55.6. <sup>11</sup>B NMR (128.3 MHz, CDCl<sub>3</sub>): δ -0.4 (t, <sup>1</sup>J<sub>BF</sub> = 29 Hz). <sup>19</sup>F NMR (376.1 MHz, CDCl<sub>3</sub>): δ -145.3 (q, <sup>1</sup>J<sub>FB</sub> = 29 Hz). FTIR (KBr): 2948 (m), 2900 (m), 2834 (m), 1641 (s), 1596 (s), 1508 (s), 1313 (m), 1249 (s), 1164 (s) cm<sup>-1</sup>. UV-vis (toluene): λ<sub>max</sub> 551 nm (ε = 25,500 M<sup>-1</sup> cm<sup>-1</sup>). Mass Spec. (EI, +ve mode): exact mass calculated for [C<sub>21</sub>H<sub>19</sub>BF<sub>2</sub>N<sub>4</sub>O<sub>2</sub>]<sup>+</sup>: 408.1569; exact mass found: 408.1576; difference: +1.7 ppm.

**Preparation of Formazanate BF<sub>2</sub> Complex 8a (Ar<sub>1</sub> = Ar<sub>5</sub> = *o*-anisole, R<sub>3</sub> = NO<sub>2</sub>).** Formazan **5a** (1.00 g, 3.04 mmol) was dissolved in toluene (250 mL) before triethylamine (2.82 g, 3.90 mL, 27.9 mmol) was added and the solution stirred for 30 min. Boron trifluoride diethyl etherate (6.44 g, 5.60 mL, 45.4 mmol) was added and the solution heated with stirring at 105 °C for 144 h at which time the solution was dark purple with a blue hue on the sides of the flask. The solution was cooled to 20 °C and poured directly onto a column containing neutral alumina. After the toluene solution was adsorbed onto the alumina, dichloromethane was used as the eluent. The crude product was isolated as a bright orange solution, which was washed with deionized water (3 × 1.00 L). The organic layer was collected, dried over MgSO<sub>4</sub>, gravity filtered, and concentrated *in vacuo* to afford **8a** as a red-orange solid. The crude solid was purified via flash column chromatography (toluene, neutral alumina, R<sub>f</sub> = 0.33) to afford **8a** as a bright orange powder. Yield = 0.163 g, 15%. Mp = 166–168 °C. <sup>1</sup>H NMR (599.5 MHz, CDCl<sub>3</sub>): δ 7.47 (t, <sup>3</sup>J<sub>HH</sub> = 8 Hz, 2H, aryl C<sub>H</sub>), 7.36 (d, <sup>3</sup>J<sub>HH</sub> = 8 Hz, 2H, aryl C<sub>H</sub>), 7.06–7.03 (m, 4H, aryl C<sub>H</sub>), 3.92 (s, 6H, OC<sub>H</sub><sub>3</sub>). <sup>13</sup>C{<sup>1</sup>H} NMR (150.8 MHz, CDCl<sub>3</sub>): δ 155.0, 132.9, 132.7, 127.3, 120.9 (2C), 112.9, 56.5. <sup>11</sup>B NMR (128.3 MHz, CDCl<sub>3</sub>): δ -1.6 (t, <sup>1</sup>J<sub>BF</sub> = 19 Hz). <sup>19</sup>F NMR (376.1 MHz, CDCl<sub>3</sub>): δ -156.0 (q, <sup>1</sup>J<sub>FB</sub> = 18 Hz). FTIR (KBr): 3035 (m), 2974 (m), 2845 (m), 1660 (m), 1587 (m), 1557 (m), 1494 (m), 1332 (m), 1260 (m), 1100 (s), 1021 (m), 814 (m), 751 (m) cm<sup>-1</sup>. UV-vis (toluene): λ<sub>max</sub> 468 nm (ε = 7,500 M<sup>-1</sup> cm<sup>-1</sup>). MS (EI, +ve mode): exact mass calculated for [C<sub>15</sub>H<sub>14</sub>BF<sub>2</sub>N<sub>5</sub>O<sub>4</sub>]<sup>+</sup>: 377.1107; exact mass found: 377.1101; difference: -1.6 ppm.

## Acknowledgements

This work was supported by the Natural Sciences and Engineering Research Council (NSERC) of Canada Discovery Grants (L. G. L. and J. B. G.), Undergraduate Student Research Award (R. R. M.), and Canada Graduate Scholarships program (S. M. B.), the University of Western Ontario, and a Petro-Canada Young Innovator Award (J. B. G.). We thank Profs. Elizabeth R. Gillies and Mark S. Workentin for access to instrumentation within their labs.

**Keywords:** Formazanate Ligands • Boron • Fluorescent Dyes • Cell Imaging • Substituent Effects

- [1] Review: D. Frath, J. Massue, G. Ulrich, R. Ziessel, *Angew. Chem. Int. Ed.* **2014**, *53*, 2290–2310.
- [2] Selected examples: a) J. F. Araneda, W. E. Piers, B. Heyne, M. Parvez, R. McDonald, *Angew. Chem. Int. Ed.* **2011**, *50*, 12214–12217; b) Y. Kubota, Y. Ozaki, K. Funabiki, M. Matsui, *J. Org. Chem.* **2013**, *78*, 7058–7067; c) G. Nawn, S. R. Oakley, M. B. Majewski, R. McDonald, B. O. Patrick, R. G. Hicks, *Chem. Sci.* **2013**, *4*, 612–621; d) C. Bonnier, D. D. Machin, O. Abdi, B. D. Koivisto, *Org. Biomol. Chem.* **2013**, *11*, 3756–3760; e) D. Frath, A. Poirel, G. Ulrich, A. De Nicola, R. Ziessel, *Chem. Commun.* **2013**, *49*, 4908–4910; f) A. Díaz-Moscoco, E. Emond, D. L. Hughes, G. J. Tizzard, S. J. Coles, A. N. Cammidge, *J. Org. Chem.* **2014**, *79*, 8932–8936; g) I.-S. Tamgho, A. Hasheminasab, J. T. Engle, V. N. Nemykin, C. J. Ziegler, *J. Am. Chem. Soc.* **2014**, *136*, 5623–5626; h) S. T. Manjare, J. Kim, Y. Lee, D. G. Churchill, *Org. Lett.* **2014**, *16*, 520–523.
- [3] Reviews: a) R. Ziessel, G. Ulrich, A. Harriman, *New J. Chem.* **2007**, *31*, 496–501; b) A. Loudet, K. Burgess, *Chem. Rev.* **2007**, *107*, 4891–4932; c) Y. Ni, J. Wu, *Org. Biomol. Chem.* **2014**, *12*, 3774–3791.
- [4] Review: N. Boens, V. Leen, W. Dehaen, *Chem. Soc. Rev.* **2012**, *41*, 1130–1172.
- [5] Selected examples: a) T. W. Hudnall, F. P. Gabbaï, *Chem. Commun.* **2008**, 4596–4597; b) A. Nierth, A. Y. Kobitski, G. U. Nienhaus, A. Jäschke, *J. Am. Chem. Soc.* **2010**, *132*, 2646–2654; c) M. A. H. Alamiry, J. P. Hagon, A. Harriman, T. Bura, R. Ziessel, *Chem. Sci.* **2012**, *3*, 1041–1048; d) S. T. Manjare, S. Kim, W. D. Heo, D. G. Churchill, *Org. Lett.* **2014**, *16*, 410–412; e) S. Raut, J. Kimball, R. Fudala, H. Doan, B. Maliwal, N. Sabnis, A. Lacko, I. Gryczynski, S. V. Dzyuba, Z. Gryczynski, *Phys. Chem. Chem. Phys.* **2014**, *16*, 27037–27042; f) X.-D. Jiang, Y. Su, S. Yue, C. Li, H. Yu, H. Zhang, C.-L. Sun, L.-J. Xiao, *RSC Adv.* **2015**, *5*, 16735–16739.
- [6] Review: A. B. Nepomnyashchii, A. J. Bard, *Acc. Chem. Res.* **2012**, *45*, 1844–1853.
- [7] Selected examples: a) A. B. Nepomnyashchii, S. Cho, P. J. Rossky, A. J. Bard, *J. Am. Chem. Soc.* **2010**, *132*, 17550–17559; b) A. B. Nepomnyashchii, M. Bröring, J. Ahrens, A. J. Bard, *J. Am. Chem. Soc.* **2011**, *133*, 8633–8645; c) M. Hesari, S. M. Barbon, V. N. Staroverov, Z. Ding, J. B. Gilroy, *Chem. Commun.* **2015**, *51*, 3766–3769; d) M. Hesari, J.-s. Lu, S. Wang, Z. Ding, *Chem. Commun.* **2015**, *51*, 1081–1084.
- [8] Selected examples: a) L. Bonardi, H. Kanaan, F. Camerel, P. Jolinat, P. Retailleau, R. Ziessel, *Adv. Funct. Mater.* **2008**, *18*, 401–413; b) T. Rousseau, A. Cravino, T. Bura, G. Ulrich, R. Ziessel, J. Roncali, *Chem. Commun.* **2009**, 1673–1675; c) H. Usta, M. D. Yilmaz, A.-J. Avestro, D. Boudinet, M. Dentí, W. Zhao, J. F. Stoddart, A. Facchetti, *Adv. Mater.* **2013**, *25*, 4327–4334; d) N. J. Findlay, J. Bruckbauer, A. R. Inigo, B. Breig, S. Arumugam, D. J. Wallis, R. W. Martin, P. J. Skabara, *Adv. Mater.* **2014**, *26*, 7290–7294; e) J. J. Chen, S. M. Conron, P. Erwin, M. Dimitriou, K. McAlahney, M. E. Thompson, *ACS Appl. Mater. Interfaces* **2015**, *7*, 662–669.
- [9] Reviews: a) S. G. Awuah, Y. You, *RSC Adv.* **2012**, *2*, 11169–11183; b) A. Kamkaew, S. H. Lim, H. B. Lee, L. V. Kiew, L. Y. Chung, K. Burgess, *Chem. Soc. Rev.* **2013**, *42*, 77–88.
- [10] Selected examples: a) A. Kamkaew, K. Burgess, *J. Med. Chem.* **2013**, *56*, 7608–7614; b) Y.-C. Lai, S.-Y. Su, C.-C. Chang, *ACS Appl. Mater. Interfaces* **2013**, *5*, 12935–12943; c) R. L. Watley, S. G. Awuah, M. Bio, R. Cantu, H. B. Gobeze, V. N. Nesterov, S. K. Das, F. D'Souza, Y. You, *Chem. Asian J.* **2015**, *10*, 1335–1343.
- [11] Review: T. Kowada, H. Maeda, K. Kikuchi, *Chem. Soc. Rev.* **2015**, *44*, 4953–4972.
- [12] Selected examples: a) T. Komatsu, Y. Urano, Y. Fujikawa, T. Kobayashi, H. Kojima, T. Terai, K. Hanaoka, T. Nagano, *Chem. Commun.* **2009**, 7015–7017; b) Y. Ueno, J. Jose, A. Loudet, C. Pérez-Bolívar, P. Anzenbacher, Jr., K. Burgess, *J. Am. Chem. Soc.* **2011**, *133*, 51–55; c) R. Hu, C. F. A. Gómez-Durán, J. W. Y. Lam, J. L. Belmonte-Vázquez, C. Deng, S. Chen, R. Ye, E. Peña-Cabrera, Y. Zhong, K. S. Wong, B. Z. Tang, *Chem. Commun.* **2012**, *48*, 10099–10101; d) T. Gayathri, A. K. Barui, S. Prashanthi, C. R. Patra, S. P. Singh, *RSC Adv.* **2014**, *4*, 47409–47413; e) J. J. Hu, N.-K. Wong, Q. Gu, X. Bai, S. Ye, D. Yang, *Org. Lett.* **2014**, *16*, 3544–3547; f) F. Wang, Y. Zhu, L. Zhou, L. Pan, Z. Cui, Q. Fei, S. Luo, D. Pan, Q. Huang, R. Wang, C. Zhao, H. Tian, C. Fan, *Angew. Chem. Int. Ed.* **2015**, *54*, 7349–7353; g) A. K. Yadav, D. L. Shen, X. Shan, X. He, A. R. Kermodé, D. J. Vocadlo, *J. Am. Chem. Soc.* **2015**, *137*, 1181–1189; h) A. Kamkaew, S. Thavornpradit, T. Puangsamlee, D. Xin, N. Wanichacheva, K. Burgess, *Org. Biomol. Chem.* **2015**, *13*, 8271–8276.
- [13] a) M.-C. Chang, E. Otten, *Chem. Commun.* **2014**, *50*, 7431–7433; b) S. M. Barbon, P. A. Reinkeluers, J. T. Price, V. N. Staroverov, J. B. Gilroy, *Chem. Eur. J.* **2014**, *20*, 11340–11344; c) S. M. Barbon, J. T. Price, P. A. Reinkeluers, J. B. Gilroy, *Inorg. Chem.* **2014**, *53*, 10585–10593; d) S. M. Barbon, V. N. Staroverov, J. B. Gilroy, *J. Org. Chem.* **2015**, *80*, 5226–5235; e) S. M. Barbon, J. T. Price, U. Yograiah, J. B. Gilroy, *RSC Adv.* **2015**, *5*, 56316–56324; M.-C. Chang, E. Otten, *Inorg. Chem.* **2015**, *54*, DOI: 10.1021/acs.inorgchem.5b01287.
- [14] Reviews: a) A. W. Nineham, *Chem. Rev.* **1955**, *55*, 355–483; b) A. S. Shawali, N. A. Samy, *J. Adv. Res.* **2015**, *6*, 241–254.
- [15] Review: M. V. Berridge, P. M. Herst, A. S. Tan, *Biotechnol. Annu. Rev.* **2005**, *11*, 127–152.
- [16] J. B. Gilroy, P. O. Otieno, M. J. Ferguson, R. McDonald, R. G. Hicks, *Inorg. Chem.* **2008**, *47*, 1279–1286.
- [17] G. I. Sigeiken, G. N. Lipunova, I. G. Pervova, *Russ. Chem. Rev.* **2006**, *75*, 885–900.
- [18] Selected examples: a) D. A. Brown, H. Bögge, G. N. Lipunova, A. Müller, W. Plass, K. G. Walsh, *Inorg. Chim. Acta* **1998**, *280*, 30–38; b) J. B. Gilroy, M. J. Ferguson, R. McDonald, B. O. Patrick, R. G. Hicks, *Chem. Commun.* **2007**, 126–128; c) J. B. Gilroy, M. J. Ferguson, R. McDonald, R. G. Hicks, *Inorg. Chim. Acta* **2008**, *361*, 3388–3393; d) J. B. Gilroy, B. O. Patrick, R. McDonald, R. G. Hicks, *Inorg. Chem.* **2008**, *47*, 1287–1294; e) S. Hong, L. M. R. Hill, A. K. Gupta, B. D. Naab, J. B. Gilroy, R. G. Hicks, C. J. Cramer, W. B. Tolman, *Inorg. Chem.* **2009**, *48*, 4514–4523; f) S. Hong, A. K. Gupta, W. B. Tolman, *Inorg. Chem.* **2009**, *48*, 6323–6325; g) M.-C. Chang, T. Dann, D. P. Day, M. Lutz, G. G. Wildgoose, E. Otten, *Angew. Chem. Int. Ed.* **2014**, *53*, 4118–4122; h) R. Travieso-Puente, M.-C. Chang, E. Otten, *Dalton Trans.* **2014**, *43*, 18035–18041; i) M.-C. Chang, P. Roewen, R. Travieso-Puente, M. Lutz, E. Otten, *Inorg. Chem.* **2015**, *54*, 379–388; j) N. A. Protasenko, A. I. Poddelsky, A. S. Bogomyakov, G. K. Fukin, V. K. Cherkasov, *Inorg. Chem.* **2015**, *54*, 6078–6080.
- [19] a) Y. A. Ibrahim, A. H. M. Elwahi, A. A. Abbas, *Tetrahedron* **1994**, *50*, 11489–11498; b) K. G. von Eschwege, G. Bosman, J. Conradie, H. Schwoerer, *J. Phys. Chem. A* **2014**, *118*, 844–855.
- [20] 2-Ethylbenzenediazonium chloride proved to be highly unstable, which resulted in an isolated yield of just 9% for 3-cyanoformazan **4d**.
- [21] W. M. Haynes, *CRC Handbook of Chemistry and Physics*, 93rd ed., CRC Press, Boca Raton, Fla, **2012**.
- [22] a) S. Fery-Forgues, D. Lavabre, *J. Chem. Educ.* **1999**, *76*, 1260–1264; b) K. Suzuki, A. Kobayashi, S. Kaneko, K. Takehira, T. Yoshihara, H. Ishida, Y. Shiina, S. Oishi, S. Tobita, *Phys. Chem. Chem. Phys.* **2009**, *11*, 9850–9860.
- [23] SAINT version 2013.2018, Bruker-AXS, **2013**, Madison, WI 53711, USA.
- [24] SADABS version 2012.2011, Bruker-AXS, **2012**, Madison, WI 53711, USA.
- [25] G. M. Sheldrick, *Acta Crystallogr.* **2015**, *A71*, 3–8.
- [26] G. M. Sheldrick, *Acta Crystallogr.* **2008**, *A64*, 112–122.

## Entry for the Table of Contents

## FULL PAPER

The evaluation of nine boron difluoride formazanate complexes bearing *o*-, *m*-, and *p*-anisole *N*-aryl substituents as readily accessible alternatives to boron dipyrromethene (BODIPY) dyes for cell imaging applications is presented. Highlights include the demonstration of the dramatic effect of anisole substitution patterns on the properties of the resulting complexes and the utility of a champion complex for fluorescence cell imaging of the cytoplasm of mouse fibroblast cells.



Ryan R. Maar, Stephanie M. Barbon,  
Neha Sharma, Hilary Groom, Leonard  
G. Luyt,\* and Joe B. Gilroy\*

Page No. – Page No.

**Evaluation of Anisole-Substituted  
Boron Difluoride Formazanate  
Complexes for Fluorescence Cell  
Imaging**

## **Table of Contents**

$^1\text{H}$ and $^{13}\text{C}$ NMR spectra.....	S2
Solid-state packing diagram for compound <b>7b</b> .....	S20
Cyclic voltammograms (oxidation and reduction).....	S20
UV-vis absorption and emission spectra.....	S22



**Figure S1.**  $^1\text{H}$  NMR spectrum of **4a** in  $\text{CDCl}_3$ . The asterisks denote residual solvent signals.

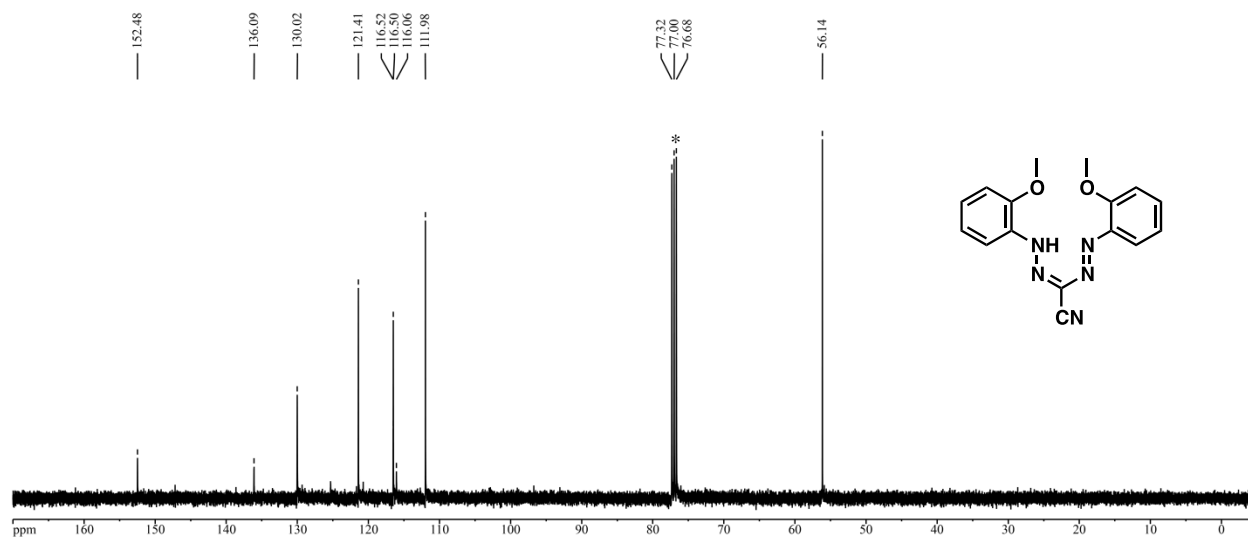


**Figure S2.**  $^{13}\text{C}\{^1\text{H}\}$  NMR spectrum of **4a** in  $\text{CDCl}_3$ . The asterisk denotes solvent signal.

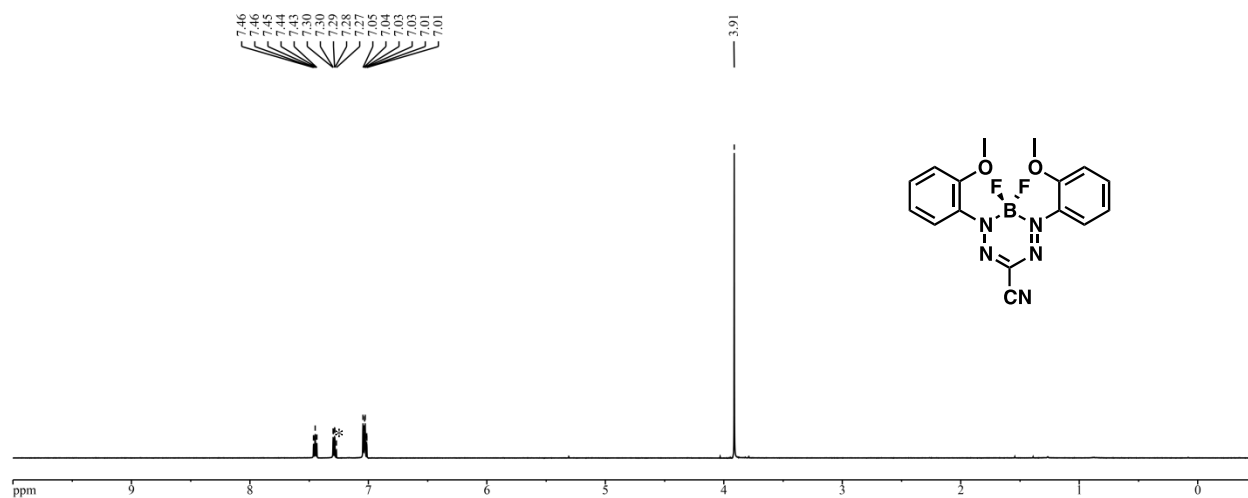


**Figure S3.**  $^1\text{H}$  NMR spectrum of **7a** in  $\text{CDCl}_3$ . The asterisk denotes residual solvent signal.

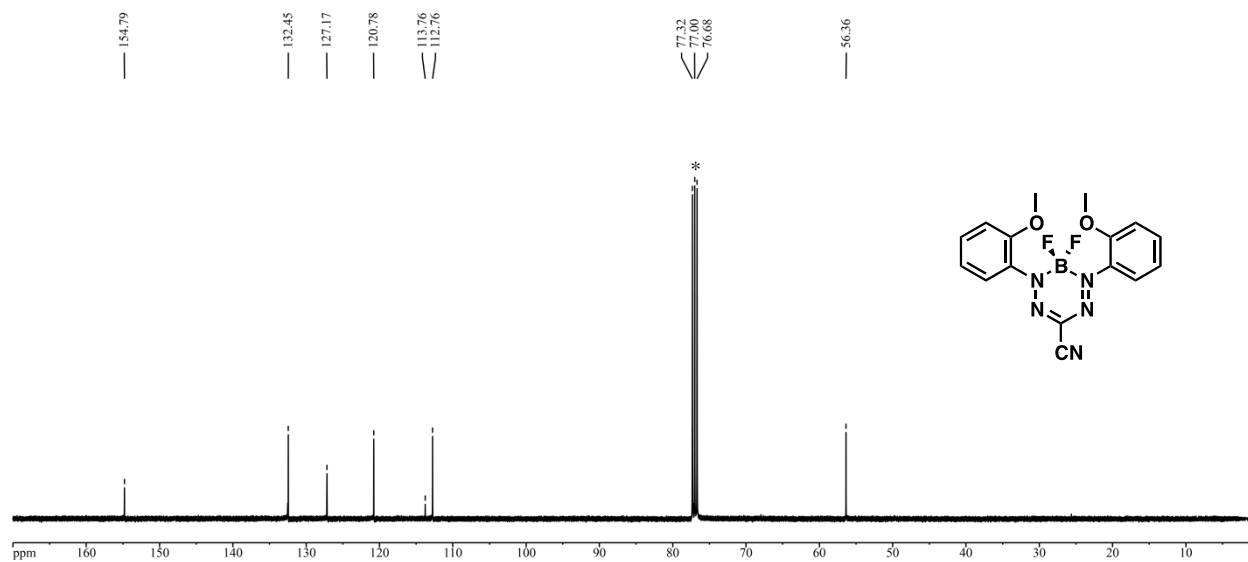


**Figure S4.**  $^{13}\text{C}\{^1\text{H}\}$  NMR spectrum of **7a** in  $\text{CDCl}_3$ . The asterisk denotes solvent signal.

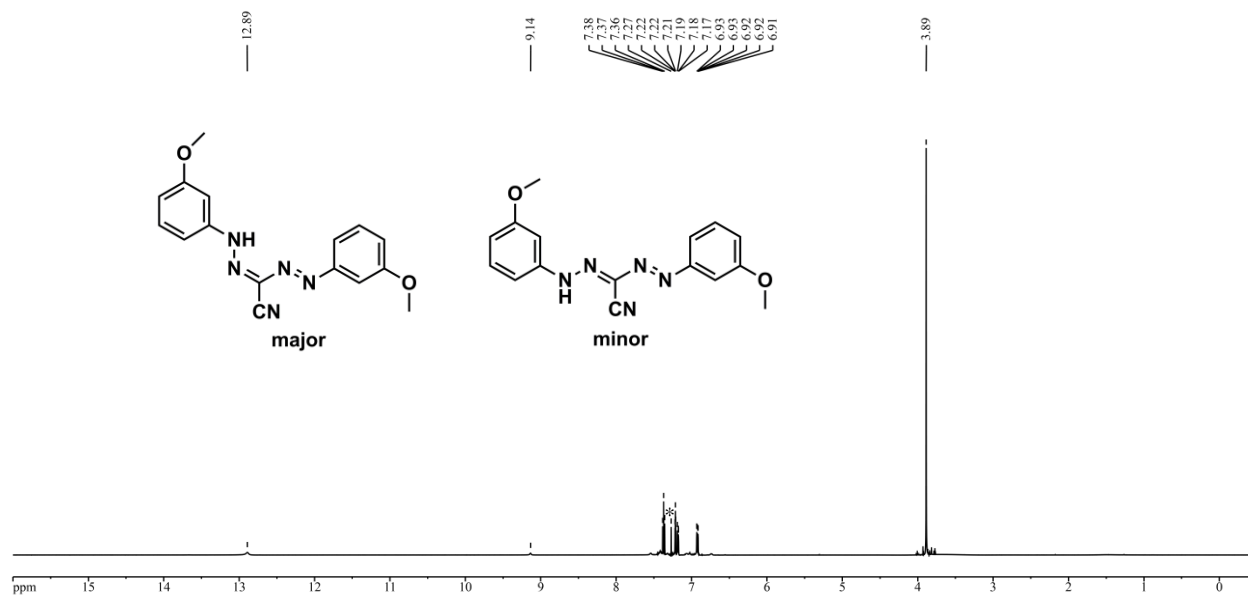


**Figure S5.**  $^1\text{H}$  NMR spectrum of **4b** in  $\text{CDCl}_3$ . The asterisk denotes residual solvent signal.

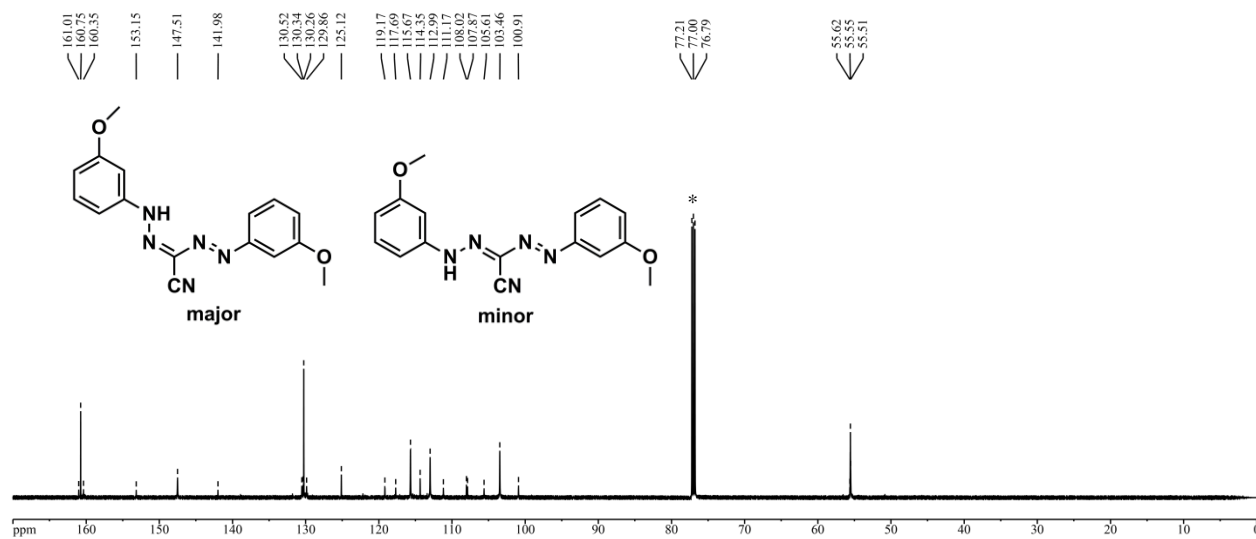


**Figure S6.**  $^{13}\text{C}\{^1\text{H}\}$  NMR spectrum of **4b** in  $\text{CDCl}_3$ . The asterisk denotes solvent signal.

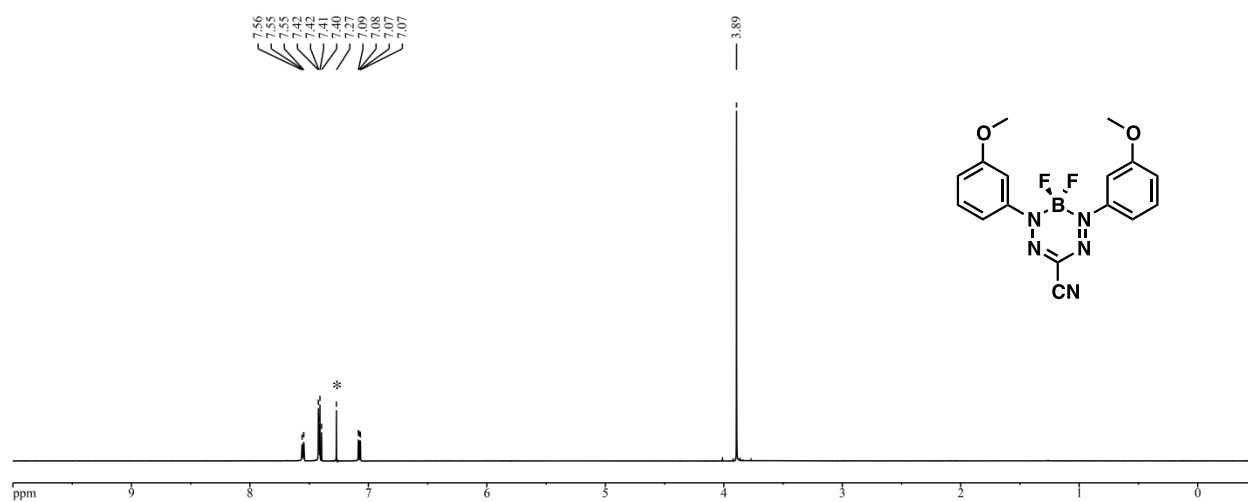


**Figure S7.**  $^1\text{H}$  NMR spectrum of **7b** in  $\text{CDCl}_3$ . The asterisk denotes residual solvent signal.

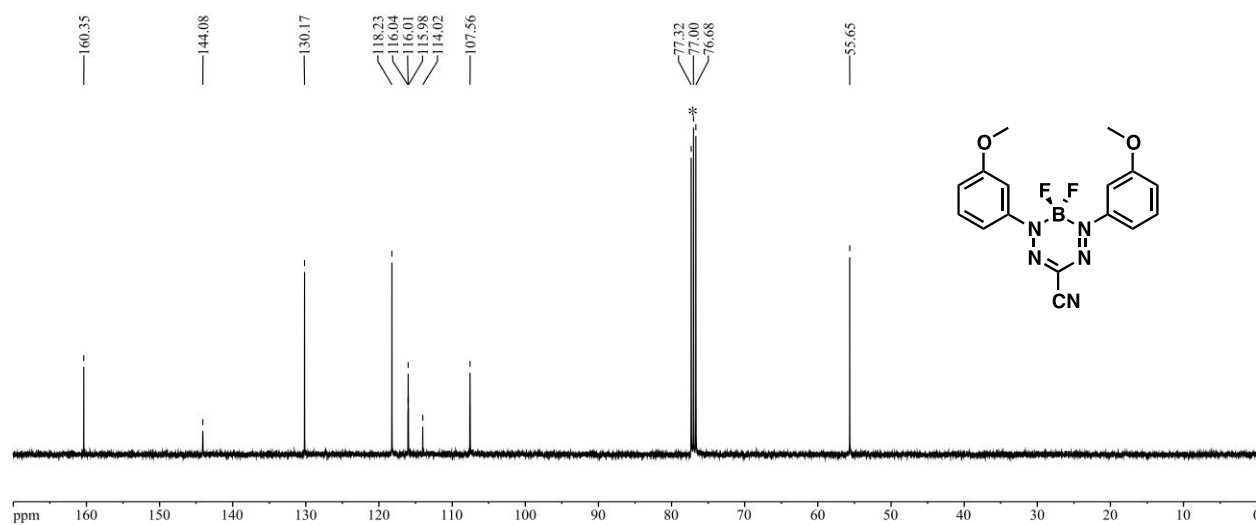


**Figure S8.**  $^{13}\text{C}\{^1\text{H}\}$  NMR spectrum of **7b** in  $\text{CDCl}_3$ . The asterisk denotes solvent signal.

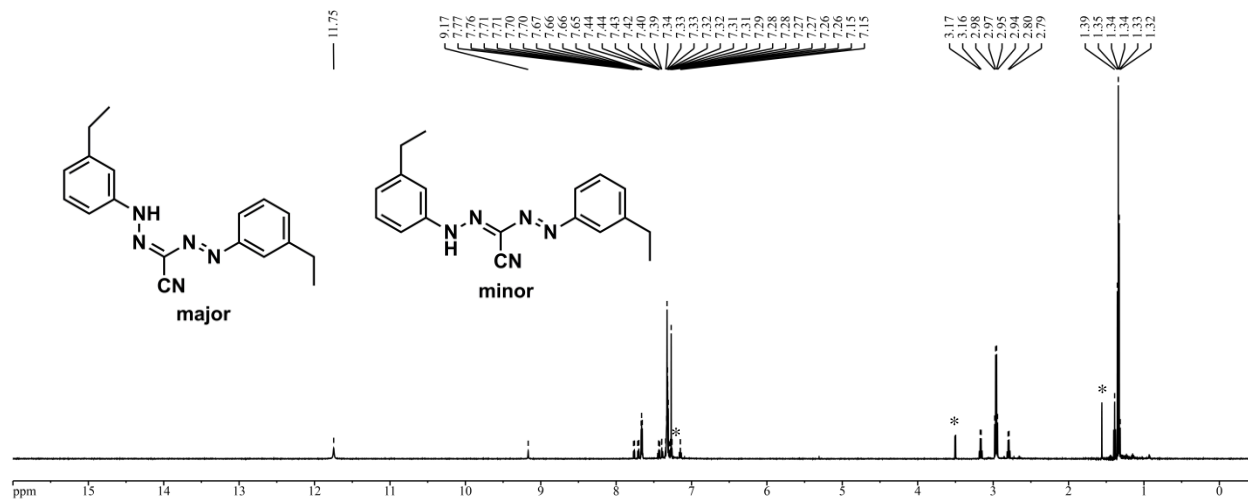


**Figure S9.**  $^1\text{H}$  NMR spectrum of **4d** in  $\text{CDCl}_3$ . The asterisks denote residual solvent signals.

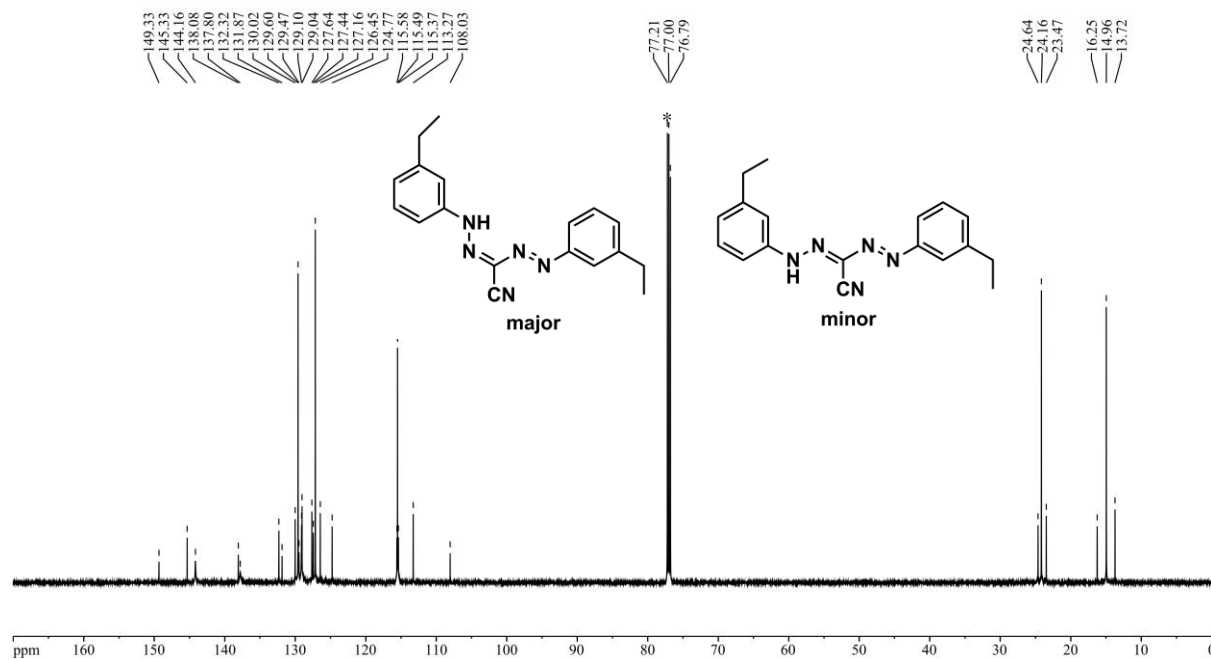


**Figure S10.**  $^{13}\text{C}\{^1\text{H}\}$  NMR spectrum of **4d** in  $\text{CDCl}_3$ . The asterisk denotes solvent signal.

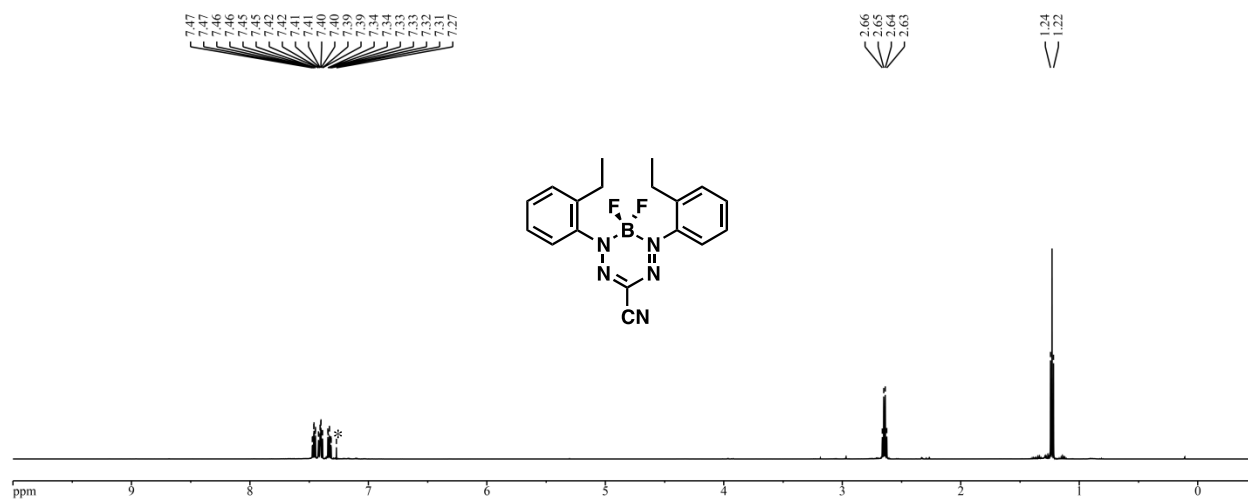


**Figure S11.**  $^1\text{H}$  NMR spectrum of **7d** in  $\text{CDCl}_3$ . The asterisk denotes residual solvent signal.

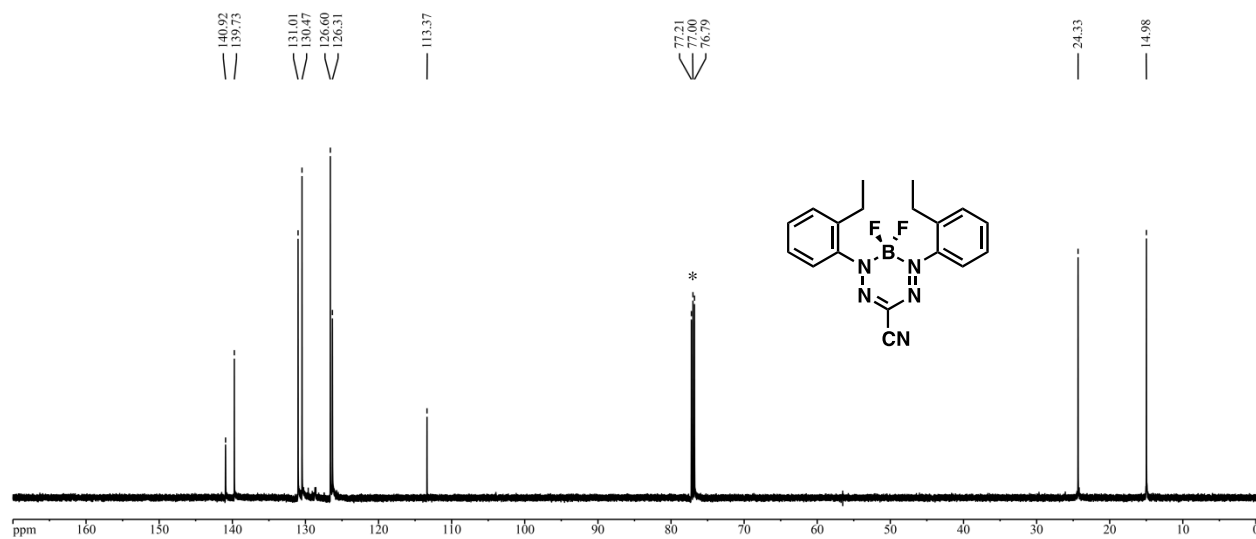


**Figure S12.**  $^{13}\text{C}\{^1\text{H}\}$  NMR spectrum of **7d** in  $\text{CDCl}_3$ . The asterisk denotes solvent signal.

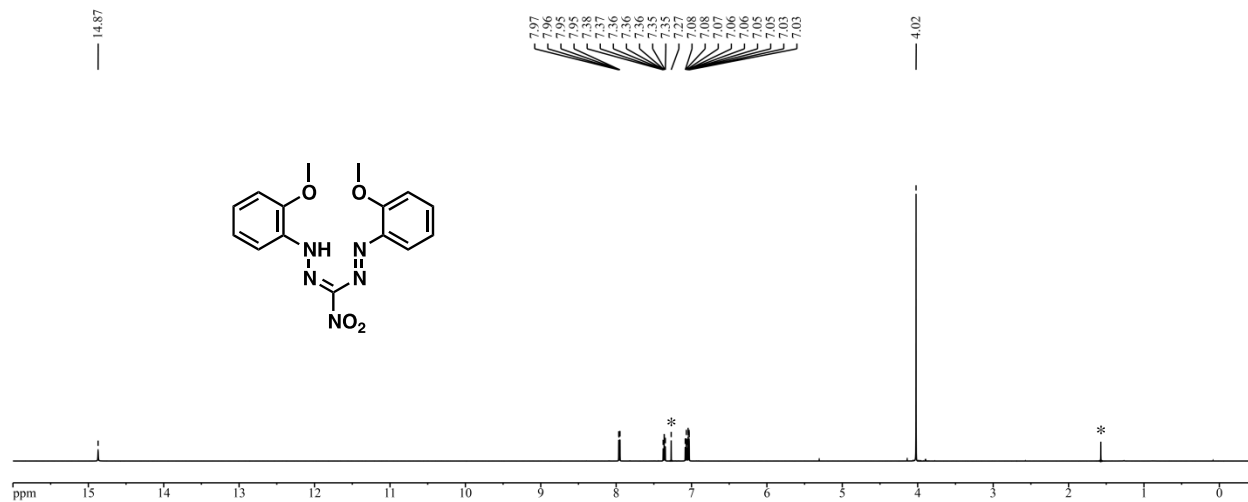


**Figure S13.** <sup>1</sup>H NMR spectrum of **5a** in CDCl<sub>3</sub>. The asterisks denote residual solvent signals.

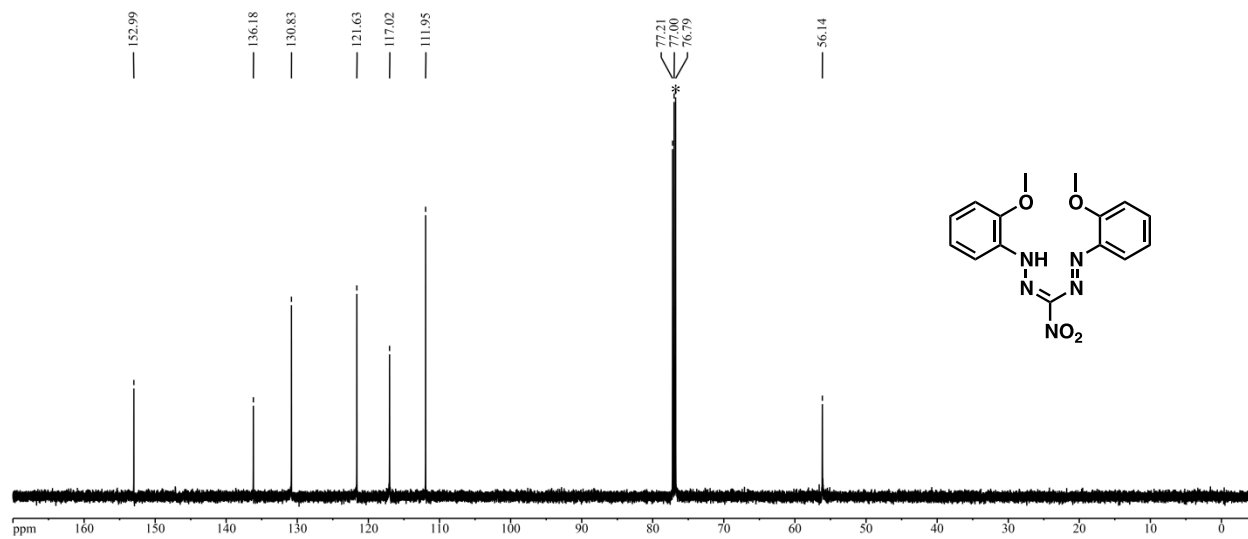


**Figure S14.** <sup>13</sup>C{<sup>1</sup>H} NMR spectrum of **5a** in CDCl<sub>3</sub>. The asterisk denotes solvent signal.

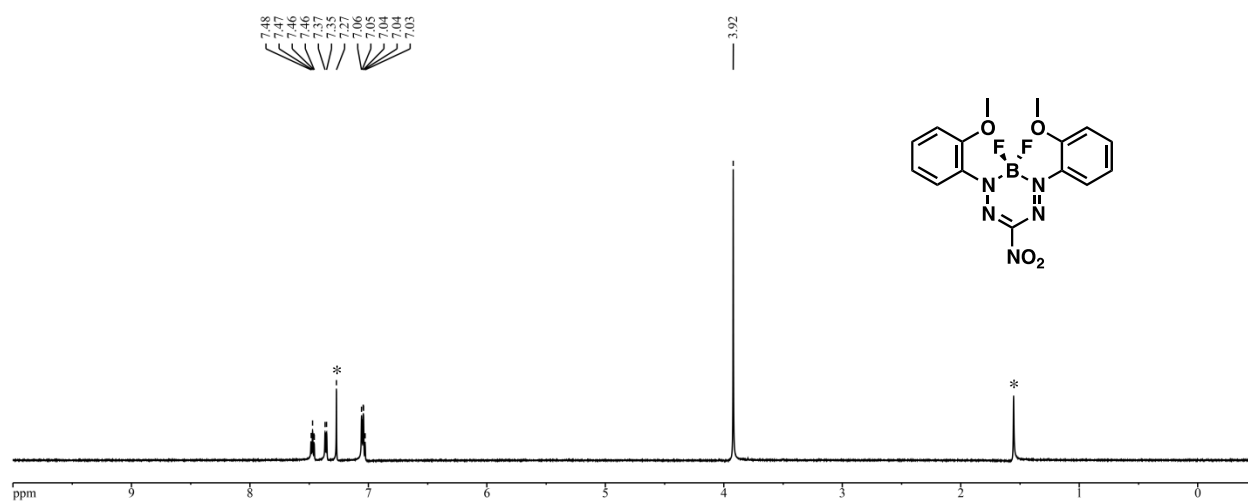


**Figure S15.**  $^1\text{H}$  NMR spectrum of **8a** in  $\text{CDCl}_3$ . The asterisks denote residual solvent signals.

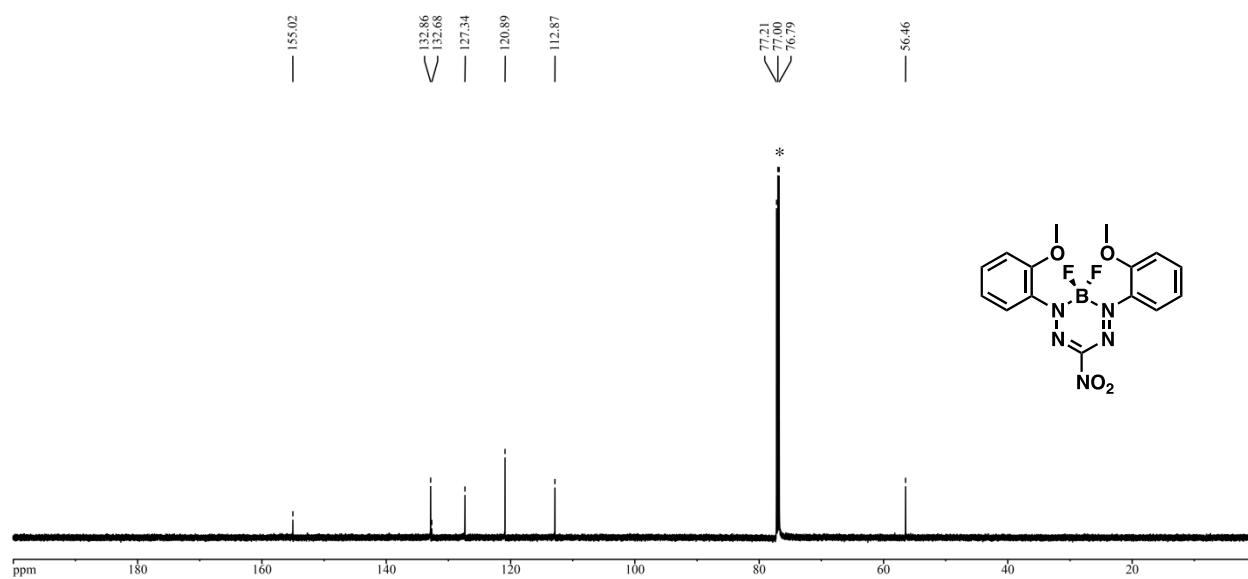


**Figure S16.**  $^{13}\text{C}\{^1\text{H}\}$  NMR spectrum of **8a** in  $\text{CDCl}_3$ . The asterisk denotes solvent signal.

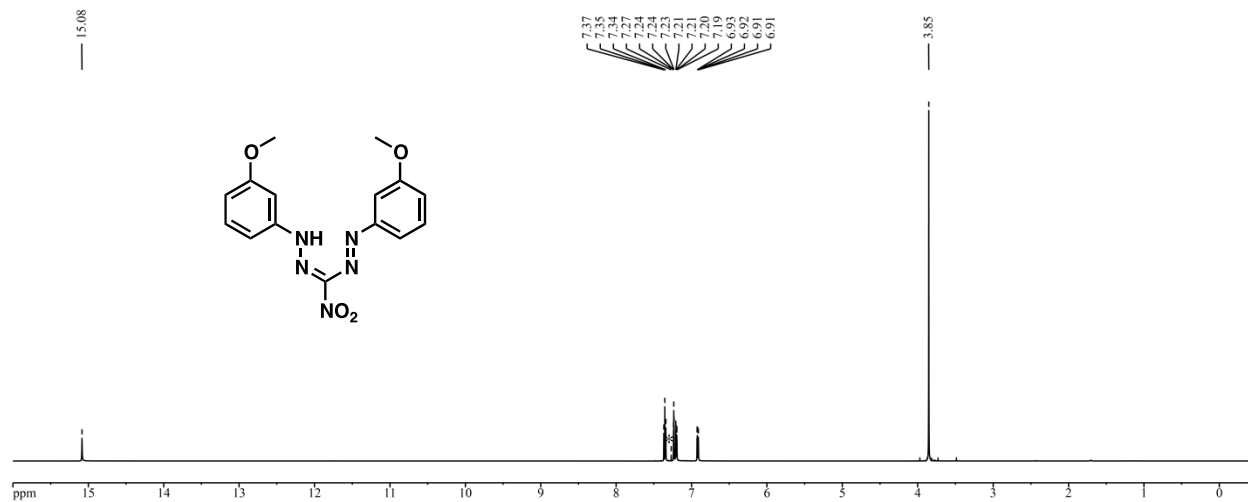


**Figure S17.**  $^1\text{H}$  NMR spectrum of **5b** in  $\text{CDCl}_3$ . The asterisk denotes residual solvent signal.

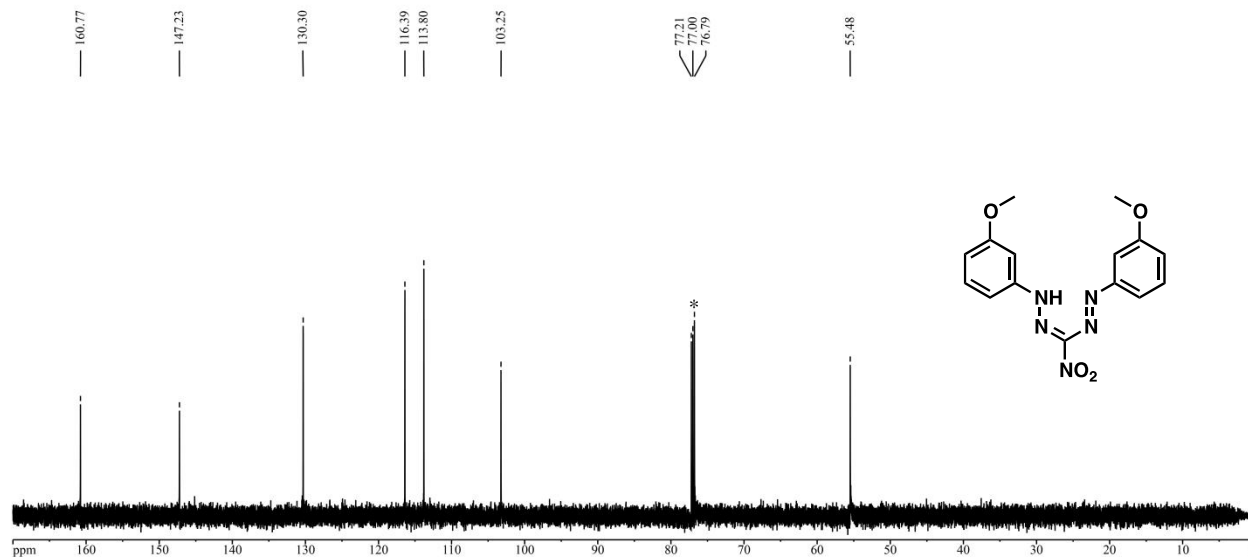


**Figure S18.**  $^{13}\text{C}\{^1\text{H}\}$  NMR spectrum of **5b** in  $\text{CDCl}_3$ . The asterisk denotes solvent signal.

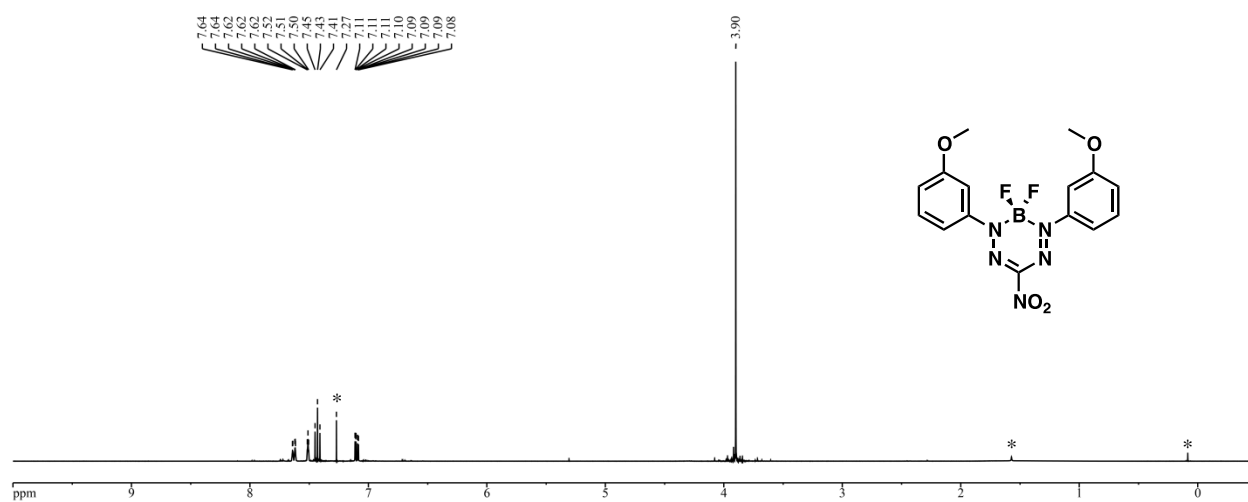


**Figure S19.**  $^1\text{H}$  NMR spectrum of **8b** in  $\text{CDCl}_3$ . The asterisks denote residual solvent signals.

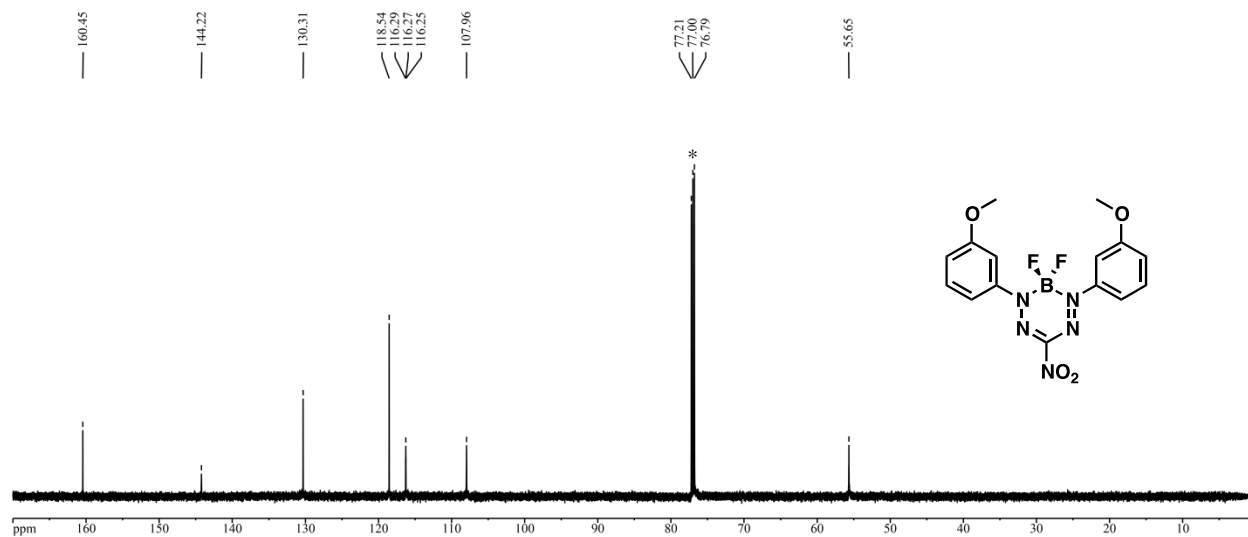


**Figure S20.**  $^{13}\text{C}\{^1\text{H}\}$  NMR spectrum of **8b** in  $\text{CDCl}_3$ . The asterisk denotes solvent signal.

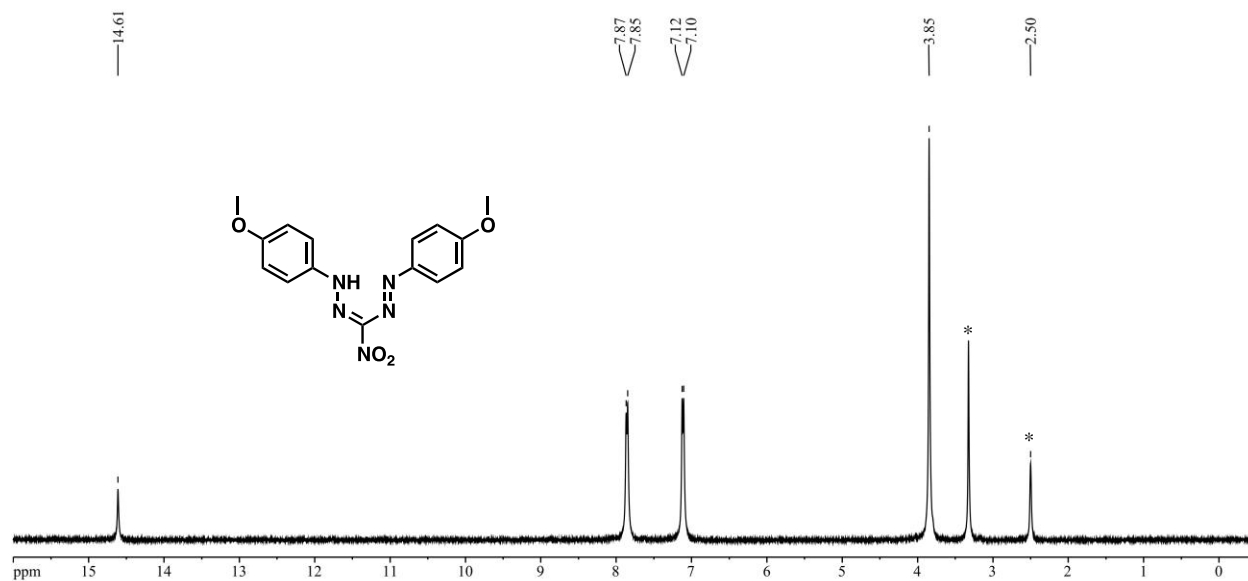


**Figure S21.**  $^1\text{H}$  NMR spectrum of **5c** in  $\text{DMSO-}d_6$ . The asterisks denote residual solvent signals.

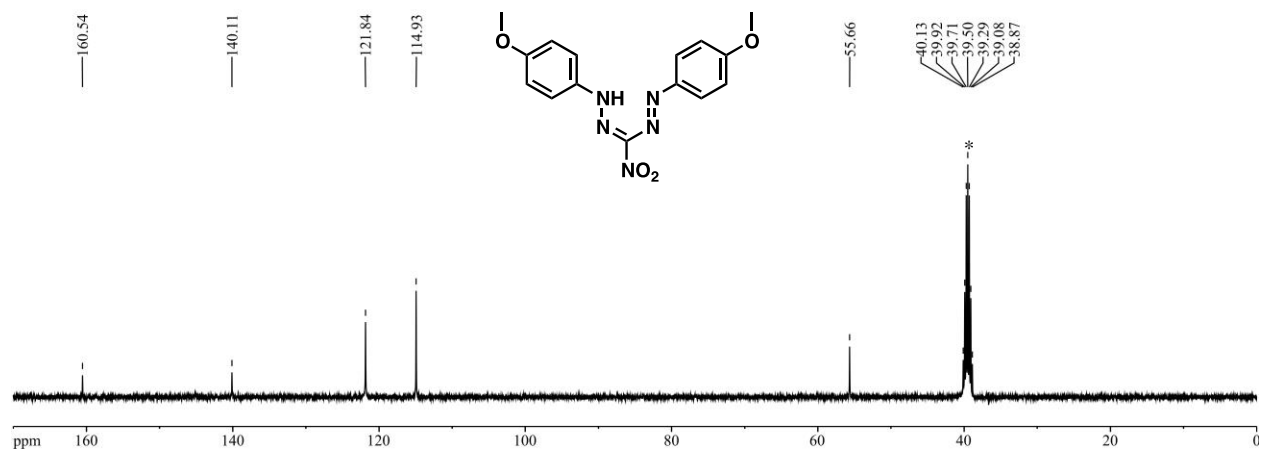


**Figure S22.**  $^{13}\text{C}\{^1\text{H}\}$  NMR spectrum of **5c** in  $\text{DMSO-}d_6$ . The asterisk denotes solvent signal.

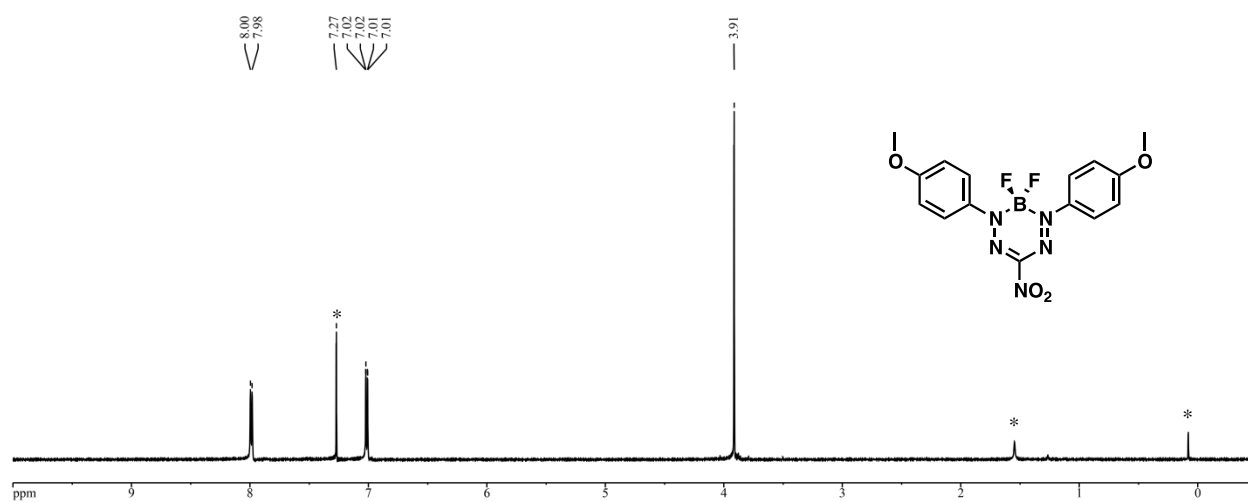


**Figure S23.**  $^1\text{H}$  NMR spectrum of **8c** in  $\text{CDCl}_3$ . The asterisks denote residual solvent signals.

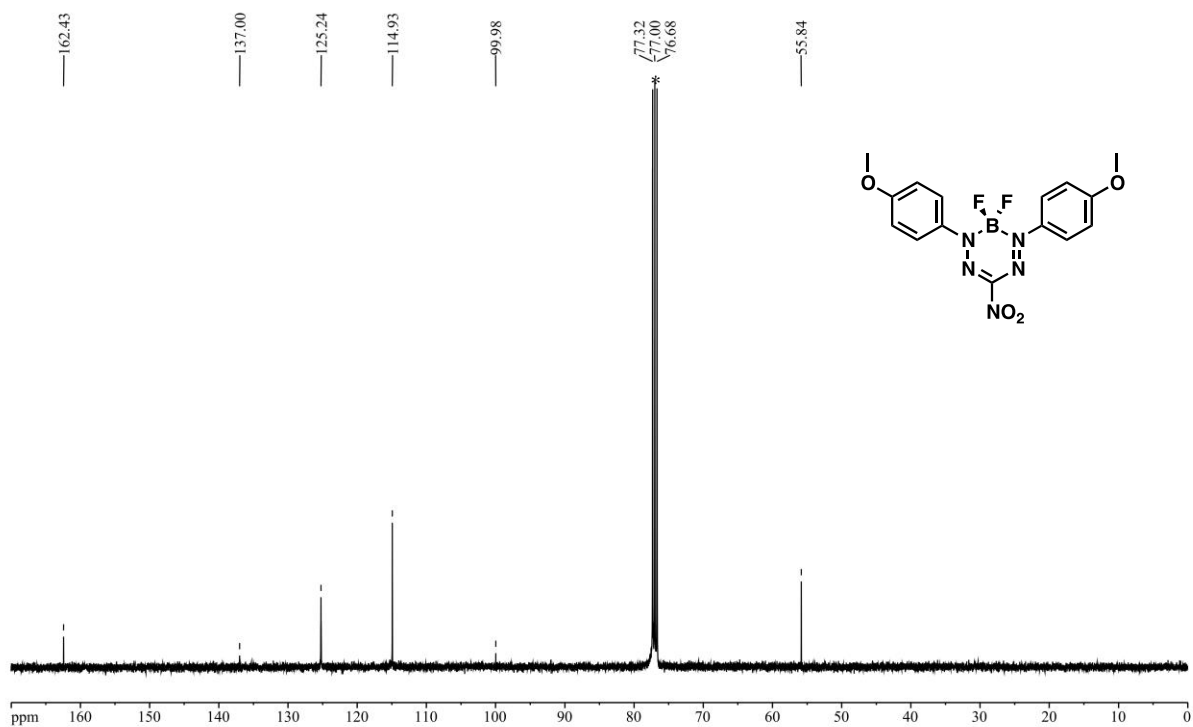


**Figure S24.**  $^{13}\text{C}\{^1\text{H}\}$  NMR spectrum of **8c** in  $\text{CDCl}_3$ . The asterisk denotes solvent signal.

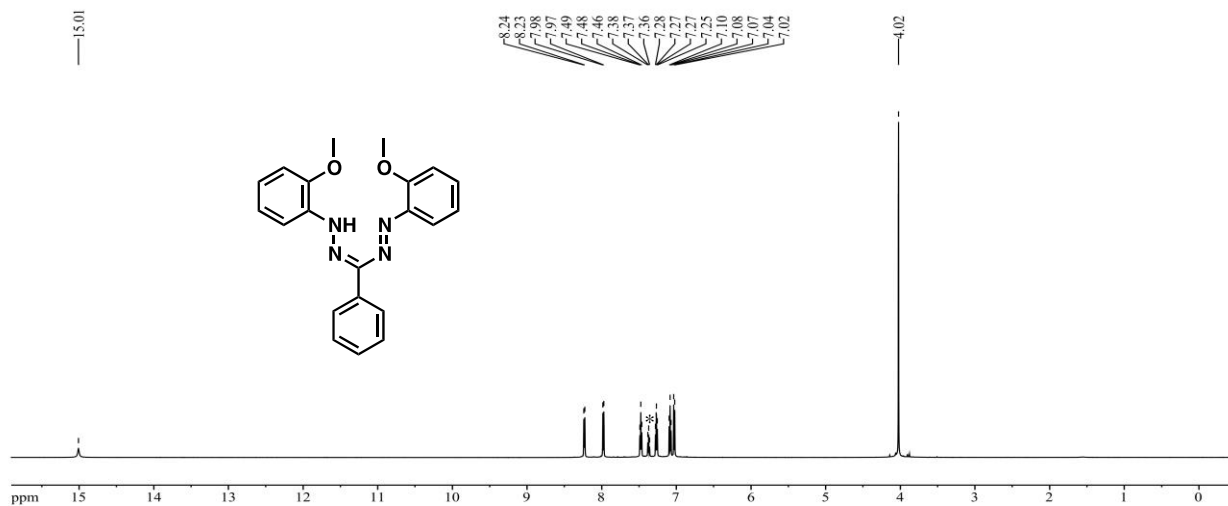


**Figure S25.**  $^1\text{H}$  NMR spectrum of **6a** in  $\text{CDCl}_3$ . The asterisk denotes residual solvent signal.

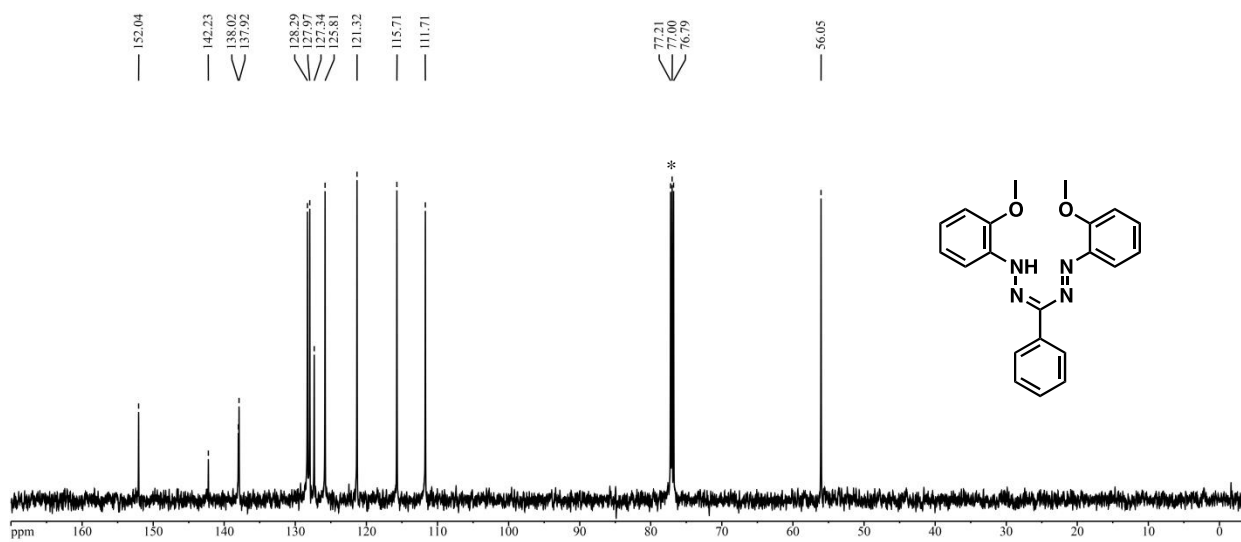


**Figure S26.**  $^{13}\text{C}\{^1\text{H}\}$  NMR spectrum of **6a** in  $\text{CDCl}_3$ . The asterisk denotes solvent signal.

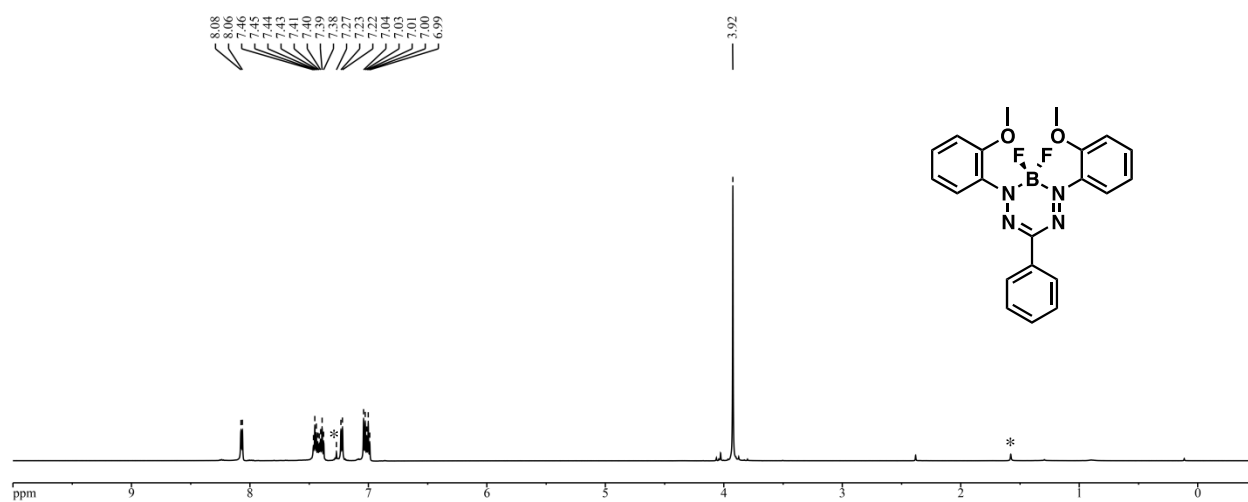


**Figure S27.**  $^1\text{H}$  NMR spectrum of **9a** in  $\text{CDCl}_3$ . The asterisks denote residual solvent signals.

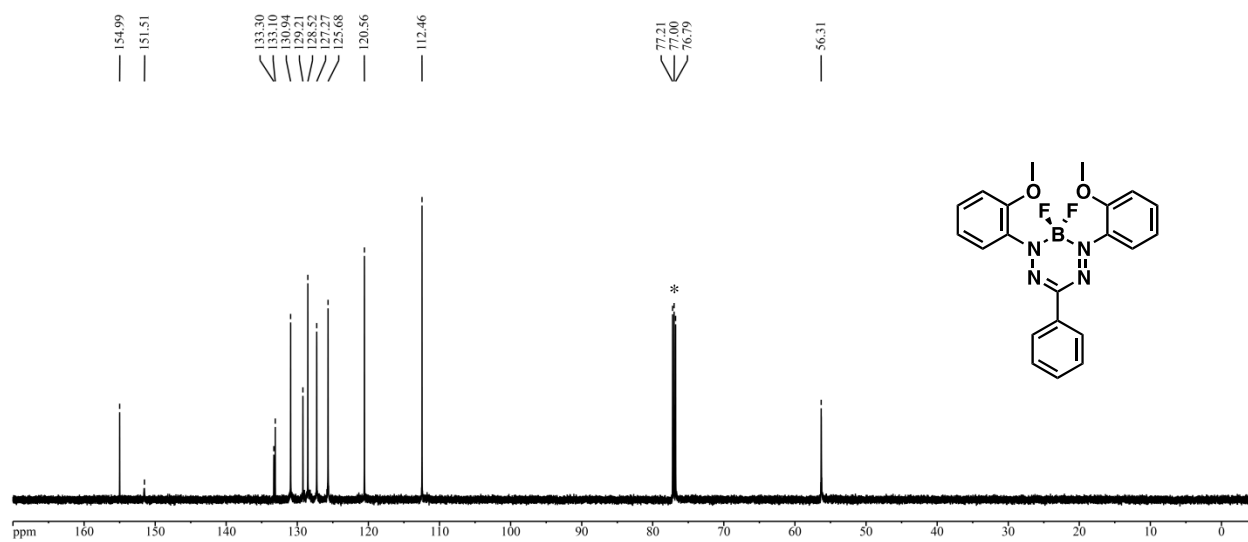


**Figure S28.**  $^{13}\text{C}\{^1\text{H}\}$  NMR spectrum of **9a** in  $\text{CDCl}_3$ . The asterisk denotes solvent signal.

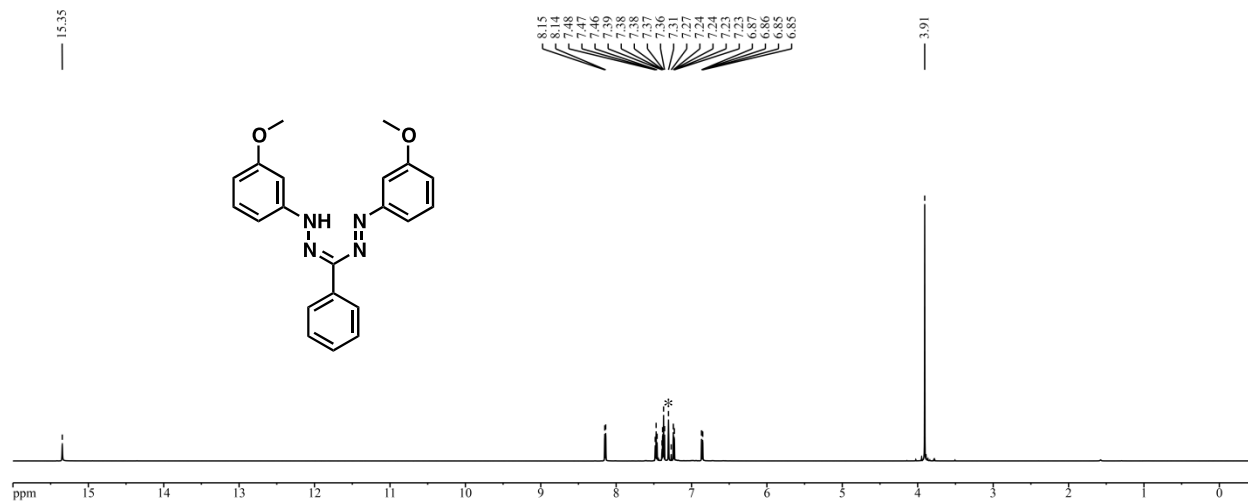


**Figure S29.**  $^1\text{H}$  NMR spectrum of **6b** in  $\text{CDCl}_3$ . The asterisk denotes residual solvent signal.

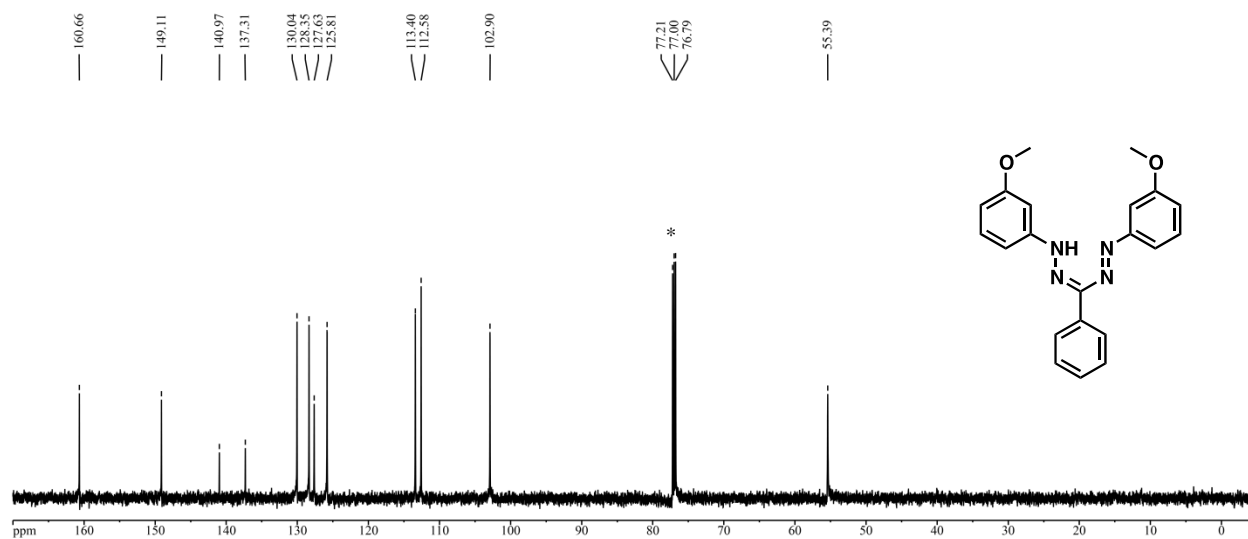


**Figure S30.**  $^{13}\text{C}\{^1\text{H}\}$  NMR spectrum of **6b** in  $\text{CDCl}_3$ . The asterisk denotes solvent signal.

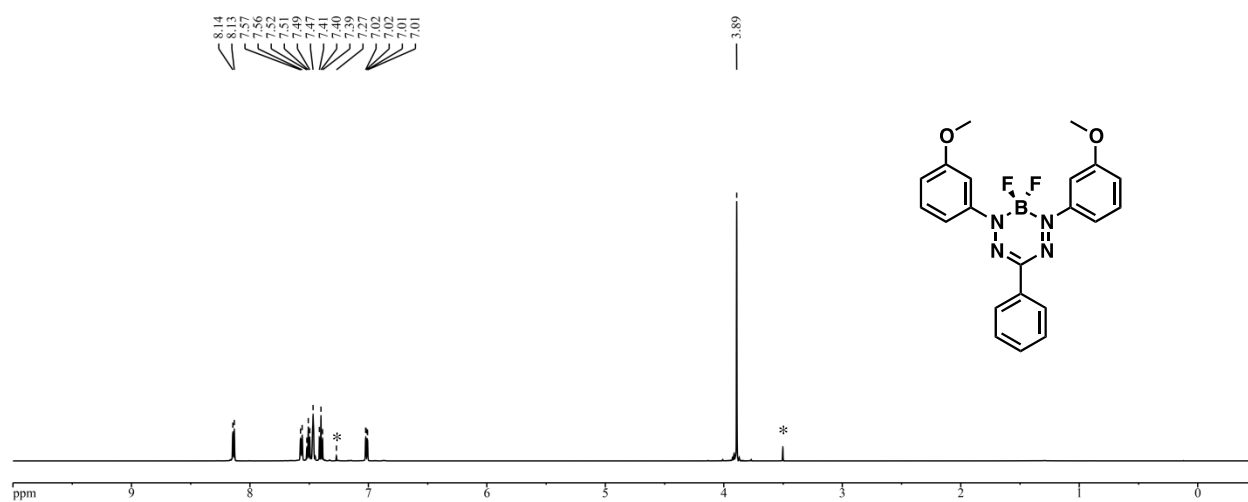


**Figure S31.** <sup>1</sup>H NMR spectrum of **9b** in CDCl<sub>3</sub>. The asterisks denote residual solvent signals.

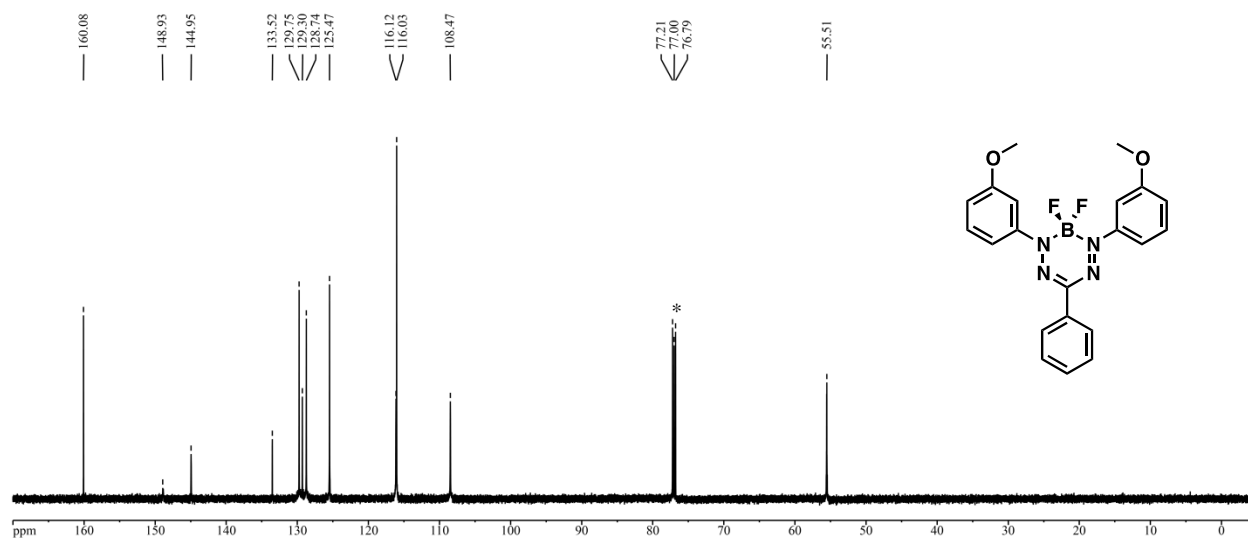


**Figure S32.** <sup>13</sup>C{<sup>1</sup>H} NMR spectrum of **9b** in CDCl<sub>3</sub>. The asterisk denotes solvent signal.

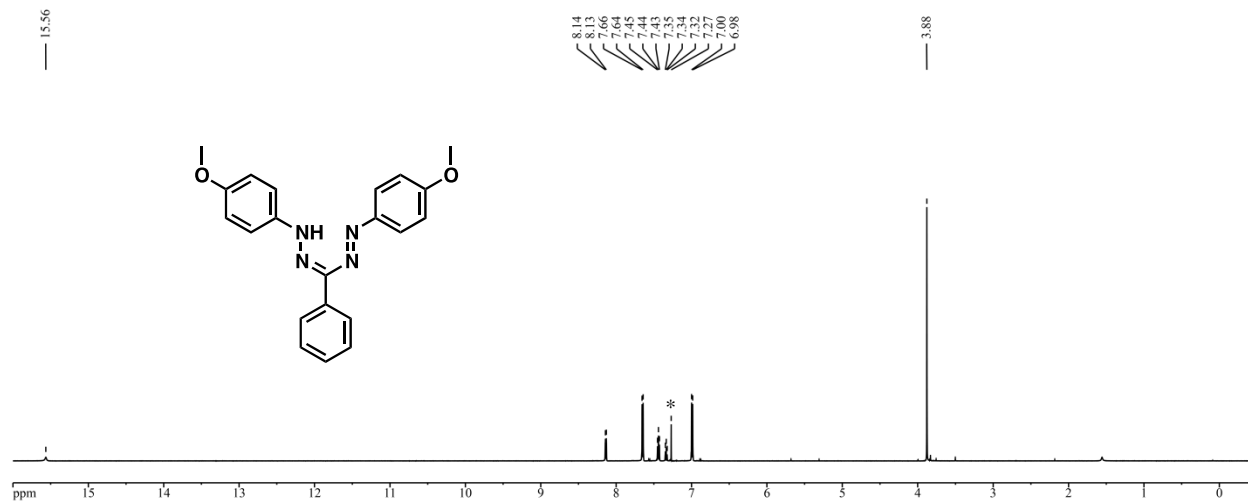


**Figure S33.**  $^1\text{H}$  NMR spectrum of **6c** in  $\text{CDCl}_3$ . The asterisk denotes residual solvent signal.

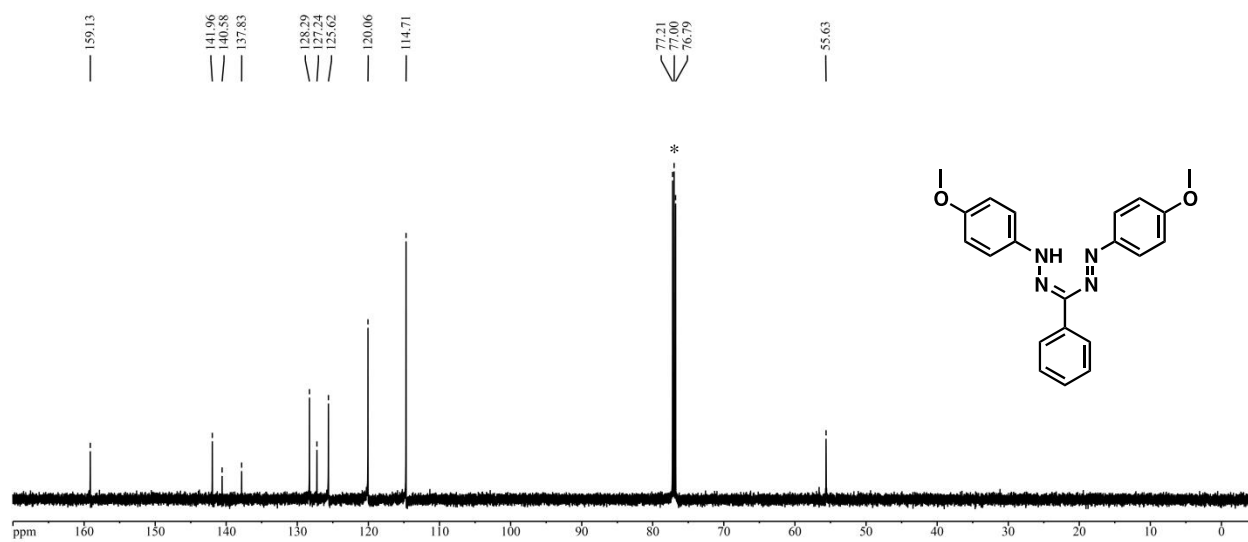


**Figure S34.**  $^{13}\text{C}\{^1\text{H}\}$  NMR spectrum of **6c** in  $\text{CDCl}_3$ . The asterisk denotes solvent signal.

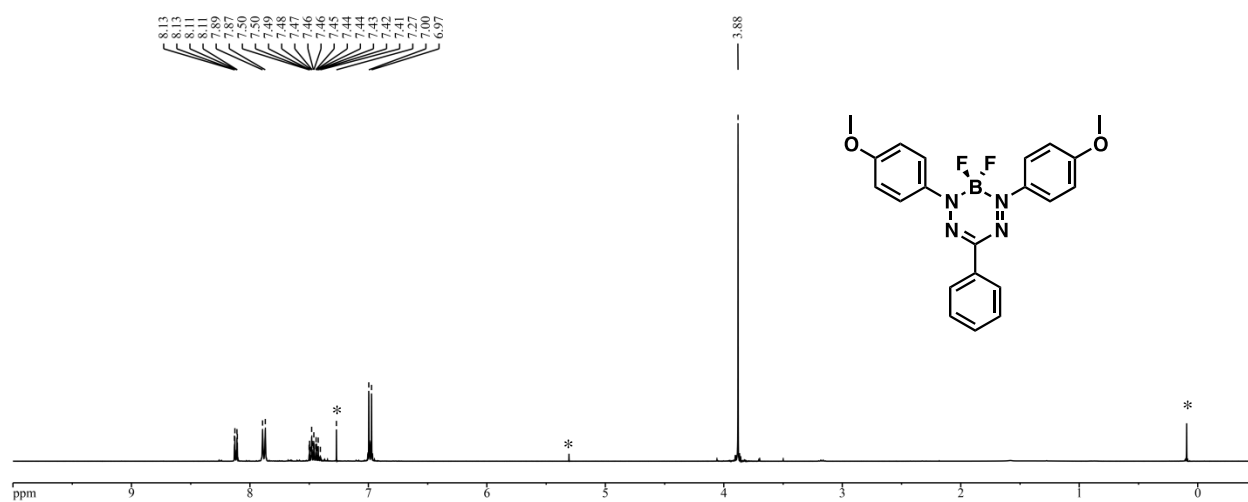


**Figure S35.**  $^1\text{H}$  NMR spectrum of **9c** in  $\text{CDCl}_3$ . The asterisks denote residual solvent and grease signals.

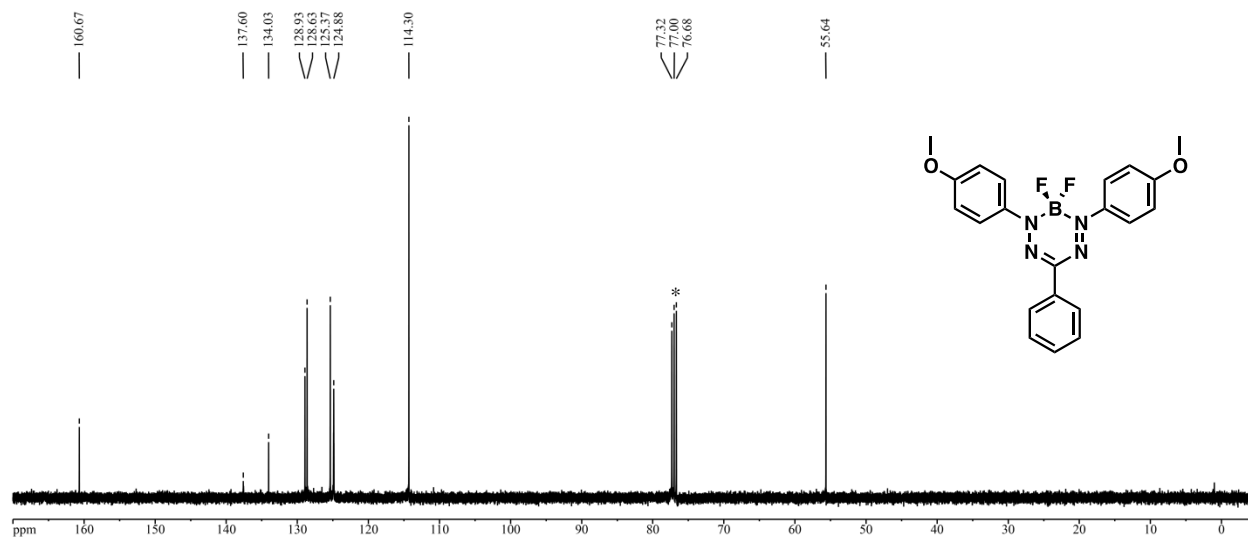


**Figure S36.**  $^{13}\text{C}\{^1\text{H}\}$  NMR spectrum of **9c** in  $\text{CDCl}_3$ . The asterisk denotes solvent signal.

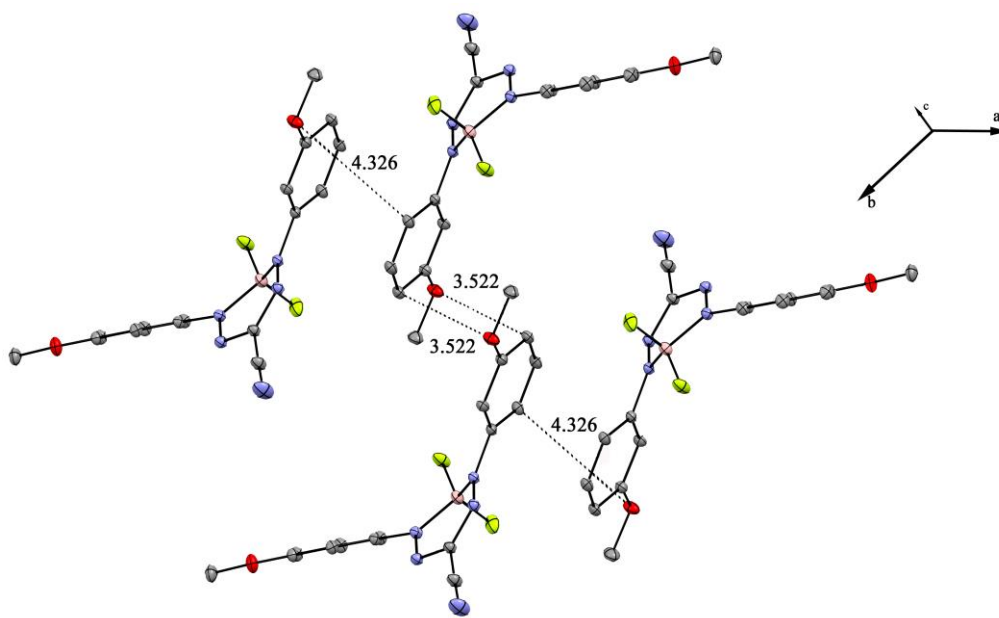


**Figure S37.** Solid-state packing of **7b**. Dashed lines indicate shortest contact points between anisole rings (Å).

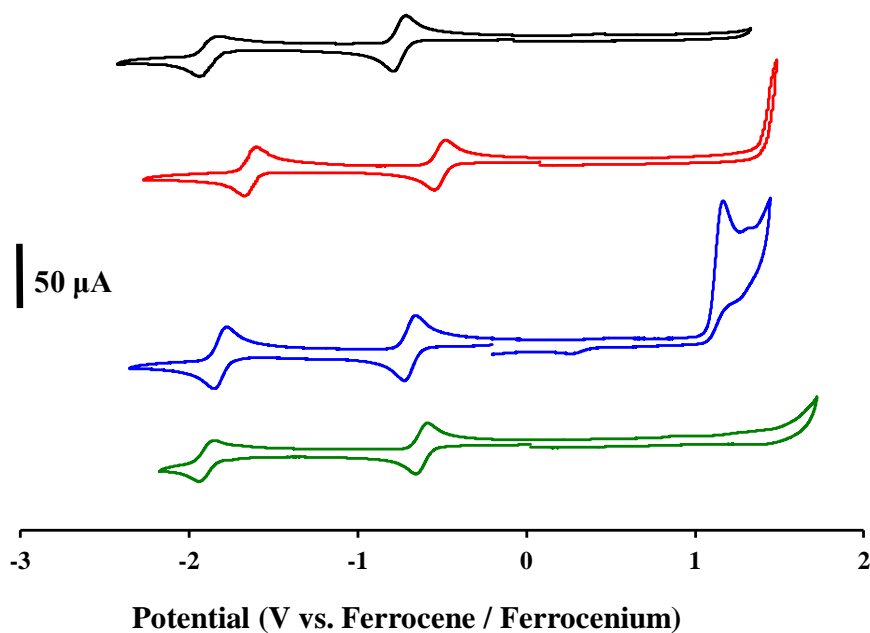


**Figure S38.** Cyclic voltammograms for  $\text{BF}_2$  formazanate complexes **7a** (Ar = *o*-anisole, R = cyano; black line), **7b** (Ar = *m*-anisole, R = cyano; red line), **7c** (Ar = *p*-anisole, R = cyano; blue line), and **7d** (Ar = *o*-ethylbenzene, R = cyano; green line) recorded in dry, degassed acetonitrile containing ~1 mM analyte and 0.1 M *n*- $\text{Bu}_4\text{NPF}_6$  at a scan rate of  $100 \text{ mV s}^{-1}$ .

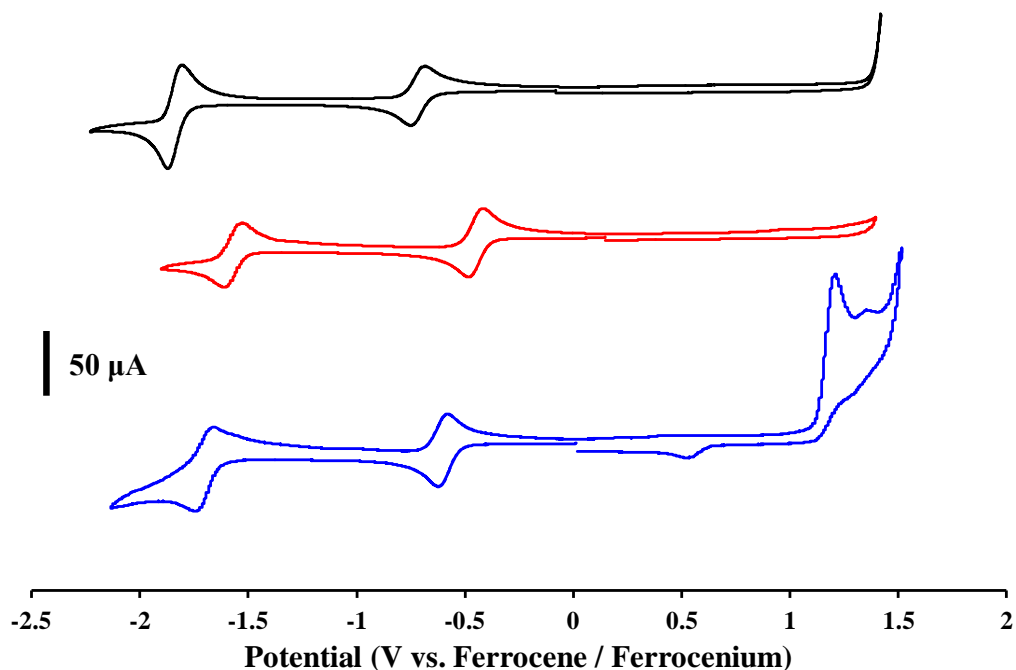


**Figure S39.** Cyclic voltammograms for BF<sub>2</sub> formazanate complexes **8a** (Ar = *o*-anisole, R = nitro; black line), **8b** (Ar = *m*-anisole, R = nitro; red line), and **8c** (Ar = *p*-anisole, R = nitro; blue line) recorded in dry, degassed acetonitrile containing ~1 mM analyte and 0.1 M *n*-Bu<sub>4</sub>NPF<sub>6</sub> at a scan rate of 100 mV s<sup>-1</sup>.

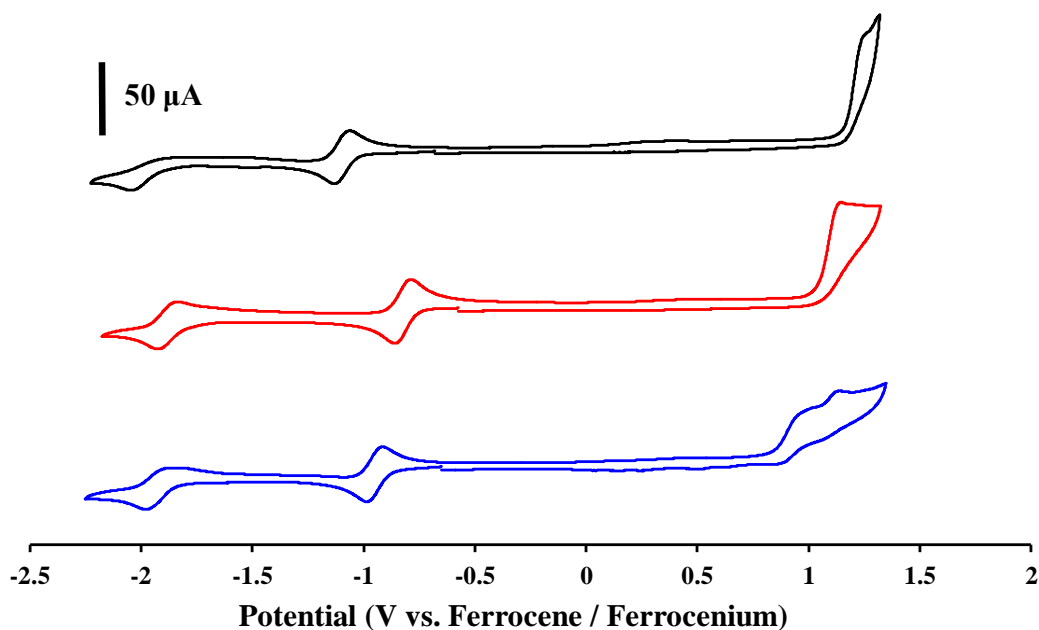


**Figure S40.** Cyclic voltammograms for BF<sub>2</sub> formazanate complexes **9a** (Ar = *o*-anisole, R = phenyl; black line), **9b** (Ar = *m*-anisole, R = phenyl; red line), and **9c** (Ar = *p*-anisole, R = phenyl; blue line) recorded in dry, degassed acetonitrile containing ~1 mM analyte and 0.1 M *n*-Bu<sub>4</sub>NPF<sub>6</sub> at a scan rate of 100 mV s<sup>-1</sup>.

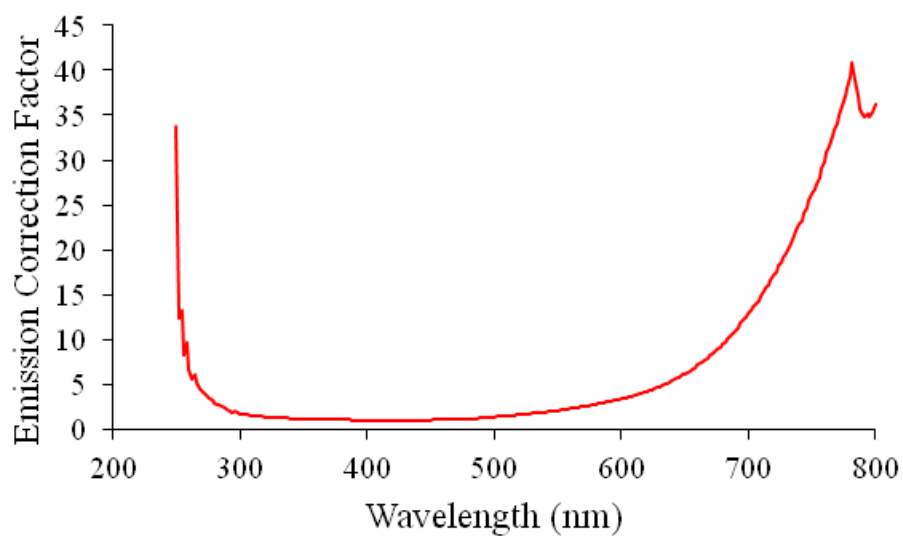


**Figure S41.** Wavelength-dependent emission correction provided by Photon Technology International.

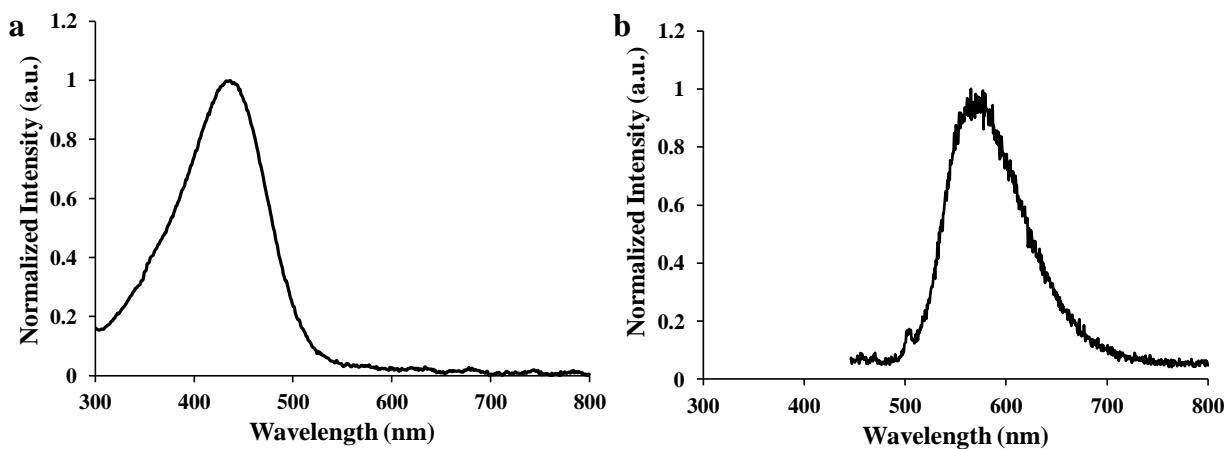


**Figure S42.** UV-vis absorption spectra (a) and emission spectra (b) for  $\text{BF}_2$  formazanate complexes **7d** ( $\text{Ar} = o$ -ethylbenzene,  $\text{R} = \text{cyano}$ ) recorded for a degassed  $10 \mu\text{M}$  toluene solution.

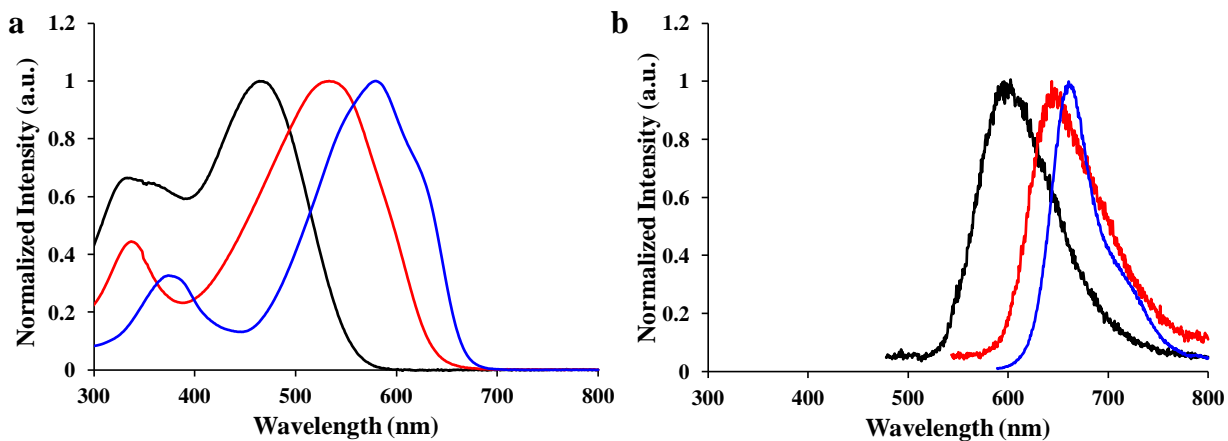


**Figure S43.** UV-vis absorption spectra (a) and emission spectra (b) for  $\text{BF}_2$  formazanate complexes **8a** (Ar = *o*-anisole, R = nitro; black line), **8b** (Ar = *m*-anisole, R = nitro; red line), and **8c** (Ar = *p*-anisole, R = nitro; blue line) recorded for degassed 10  $\mu\text{M}$  toluene solutions.

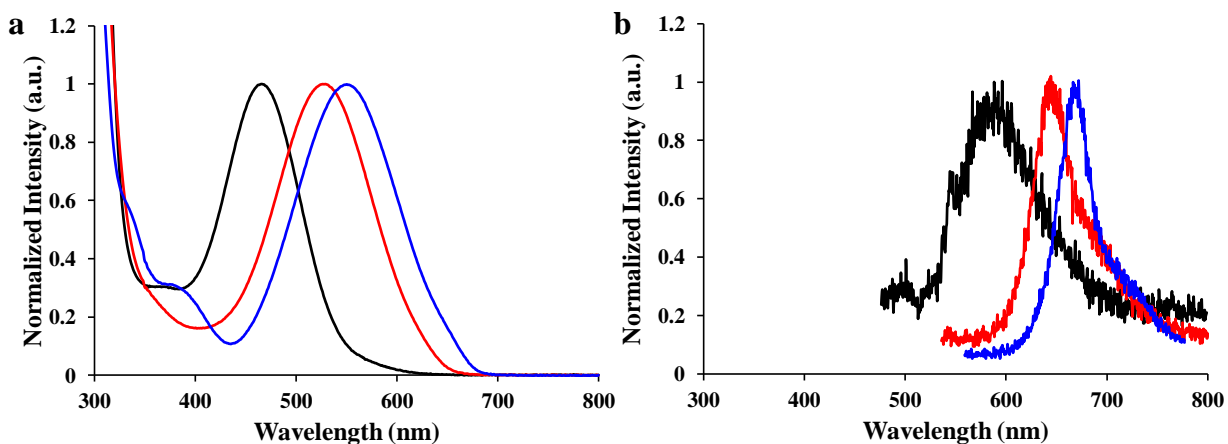


**Figure S44.** UV-vis absorption spectra (a) and emission spectra (b) for  $\text{BF}_2$  formazanate complexes **9a** (Ar = *o*-anisole, R = phenyl; black line), **9b** (Ar = *m*-anisole, R = phenyl; red line), and **9c** (Ar = *p*-anisole, R = phenyl; blue line) recorded for degassed 10  $\mu\text{M}$  toluene solutions.

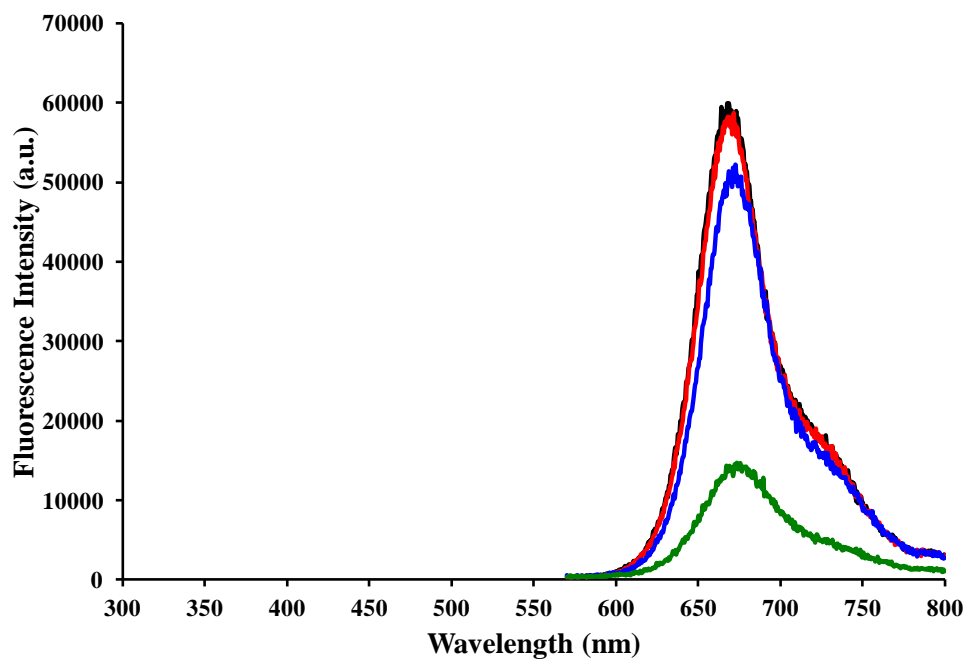


**Figure S45.** UV-vis emission spectra for BF<sub>2</sub> formazanate complexes **9c** (Ar = *p*-anisole, R = phenyl) recorded for degassed 10 μM tetrahydrofuran/water solutions containing 10% (black line), 25% (red line), 50% (blue line), and 75% (green line) v/v water.